

ISSN 0737-5352-85

ORBITING CARBON OSERVATORY (OCO)
ALGORITHM THEORETICAL BASIS DOCUMENT

THE OCO SIMULATOR

D. M. O'Brien, Igor Polonsky, Chris O'Dell, Adam Carheden
Cooperative Institute for Research in the Atmosphere
Colorado State University

2009-08-13



Contents

1	Introduction	3
2	Orbits, geometry and polarization	4
2.1	Target mode	5
2.2	Slit misalignment and polarization angle	9
3	Meteorology and trace gas profiles	12
4	Cloud optical properties	13
4.1	Liquid water cloud	13
4.2	Ice water cloud	14
5	Aerosol optical properties	15
5.1	Simple aerosol model	15
5.2	Calipso aerosol model	15
5.3	Calipso aerosol models and their particle size distribution functions	16
6	Surface properties	19
7	Radiative transfer	20
7.1	Spectroscopy and gas absorption	20
7.2	Rayleigh scattering	21
7.3	Composite atmospheric optical properties	21
7.4	Surface optical properties	22
7.5	High-resolution radiative transfer	22
7.6	Low-streams interpolator	22
7.7	Detection by the instrument	25
8	Using the simulator	27
8.1	Shared input data in <code>dat_share</code>	28
8.2	Customized input data in <code>dat_local</code>	31
8.3	Distributing the simulator over the OCO cluster at CSU	43
9	Acknowledgements	45

1 Introduction

The measurements of X_{CO_2} ¹ by NASA’s Orbiting Carbon Observatory (OCO) require unprecedented accuracy for a passive remote sensing mission, necessitating a complex retrieval algorithm that must account for gaseous absorption, scattering by clouds and aerosols, reflection by anisotropic land and ocean surfaces, polarization, realistic meteorology and trace gas profiles. Although the OCO instrument was characterized rigorously in the thermal vacuum chamber at JPL, an airborne prototype was never built. Instead it was decided by NASA that development and verification of the retrieval algorithms could be conducted within the virtual world of numerical simulations. This decision placed enormous pressure on the algorithm team to provide simulations of OCO spectra that would capture the spatial and temporal scales of variability likely to be observed by OCO. In addition, the simulations had to address the vagaries of a real instrument, including effects such as misalignment of the three spectrometers, measured instrument line shape functions and dispersion relations, and Doppler shifts caused by relative motion of the sun and satellite towards the target on the rotating earth. The output from the simulations had to be functionally identical to the L1B data stream that would be produced by the software of the ground data system. Finally, and very importantly, the simulations had to be not only accurate but fast, to enable whole orbits of high resolution spectra to be simulated on a modest-sized cluster. The simulator outlined in this report meets these challenges.

The OCO simulator draws upon both measurements and models to create synthetic L1B data files for OCO. There are three principal modes of operation.

- (1) The orbit of OCO is simulated and spectra are calculated at the OCO target using:
 - (a) cloud data from CloudSat;
 - (b) aerosol data from Calipso;
 - (c) surface properties from MODIS;
 - (d) CO₂ profiles from the Parameterized Chemical Transport Model (PCTM);
 - (e) meteorology from ECMWF analyses.

The geometry (meaning zenith angles and azimuths of the sun and satellite as seen from the OCO target) is calculated using orbital models for the sun and satellite in nadir, glint and target modes. Thus, the geometry will vary along the orbit. In this mode, the cloud, aerosol, CO₂, surface and meteorology fields are synchronized, so the spectra should represent the ‘real world’.

- (2) Rather than using simultaneous CloudSat, Calipso and ECMWF data, the simulator can draw upon a static data base of ECMWF profiles (Chevallier, 2001) to estimate the meteorological and cloud profiles.
- (3) The simulator also can be used in a mode where selected physical variables are frozen, and profiles are extracted from either the CloudSat repository or the static ECMWF data base. For example, the geometry, surface pressure and surface properties may

¹ X_{CO_2} denotes the column averaged, dry air mole fraction of CO₂.

be fixed, either as a group or individually. This mode is designed for use in training the AOPD correlation algorithm (Polonsky and O’Brien, 2009).

The sections below describe the algorithms and sources of data employed by the simulator, outlining for each the assumptions, limitations and rationale guiding the development. The final section provides a user’s guide to the simulator, including its deployment on a linux cluster using message passing interface (MPI) code.

2 Orbits, geometry and polarization

The simulator runs on the satellite clock. At each tick of the clock, the positions and velocities of the sun and satellite are computed in geocentric coordinates, and the target is located on the surface of the earth (assumed ellipsoidal). In nadir mode, the target is assumed to be the point on the surface where the local normal vector points to the satellite position. In glint mode, a bisection algorithm is used to find the point on the surface where the rays to the sun and satellite make equal angles with the local normal vector, and where all three vectors are coplanar. In target mode the satellite executes a manoeuvre to point always at the same position on the surface. For each mode, the simulator computes the polarization measured by OCO, a task that requires not only the satellite position but also its orientation in space. The simulator models the misalignments between the slits of the three OCO spectrometers, predicting for each the target position, the viewing and illumination geometries, and the angle that characterizes the polarization. Lastly, the velocities of the sun and satellite towards the target on the rotating earth are calculated and used to compute Doppler shifts, which must be treated accurately for a high resolution instrument such as OCO.

The orbit predictor is a moderate precision predictor, and has been used operationally to track satellites in an automated direct reception station at CSIRO Atmospheric Research in Australia. It uses perturbation theory accurate to second-order in the harmonic expansion of the earth’s gravitational field (Brouwer, 1959), but does not include any of the drag terms that are essential for a high precision predictor. To this degree of approximation, the orbits are elliptical, but the right ascension of the ascending node and the argument of the perigee precess at constant rates. Those rates are determined by the perturbation theory. In addition, the code allows adjustments to ensure that the orbit is strictly sun-synchronous and that the orbits repeat exactly after a specified period. For the purpose of simulating OCO spectra, however, these refinements are nice but inessential. The important feature of the predictor (and the real reason for using it) is that, in combination with a model for the orientation of the satellite, it allows the target position to be calculated for all modes, simultaneously predicting the polarization angle, and taking into account the subtle effects caused by misalignment of the slits of the three spectrometers.

This section focuses only on two aspects of the geometrical calculations, target mode and the complications caused by slit misalignment. The other features of the simulator are sufficiently standard that they may be omitted. Some details, including an analytical derivation of the target position on an ellipsoidal earth, may be found in the paper by O’Brien and Prata (1990) for the Along Track Scanning Radiometer (ATSR).

2.1 Target mode

This subsection documents the geometric calculations required to simulate OCO’s target mode. The simulator does not model the dithering of the satellite over the target; instead it models a satellite that stares at the surface during the overpass, and computes the combinations of Stokes’ parameters measured by the spectrometers.

The simulator predicts for every frame the position and velocity of the satellite, as well as the positions of the sub-satellite point and the point of specular reflection. For both nadir and glint mode, the satellite is oriented so that the vector from the target to the sun lies in the plane defined by the satellite X - and Z -axes.² In target mode, generally the observations are not made in the principal plane, so the polarization component selected by the spectrometers is a mixture of the I , Q and U components of Stokes’ vector. This subsection outlines the steps required to compute the contributions of I , Q and U .

Geometry of target mode

We make the following assumptions.

- (1) The yaw of the satellite is maintained as the satellite moves into and through target mode. For the purpose of the simulator we assume that the initial yaw is zero. Therefore, throughout the sequence of observations in target mode, the satellite Z -axis will lie in the plane containing the satellite position and velocity vectors.
- (2) The satellite $-X$ -axis points to the target.
- (3) The spectrometer slits are parallel to the satellite Y -axis.
- (4) The polarizer transmits light whose plane of polarization contains the Y -axis.

Let \mathbf{u} denote a unit vector pointing from the centre of the earth to the satellite, and let \mathbf{t} denote a unit vector parallel to the satellite velocity. Define \mathbf{v} to be a unit vector orthogonal to \mathbf{u} in the plane defined by \mathbf{u} and \mathbf{t} with

$$\mathbf{t} \cdot \mathbf{v} > 0,$$

and then define

$$\mathbf{w} = \mathbf{u} \times \mathbf{v}.$$

The vectors \mathbf{u} , \mathbf{v} and \mathbf{w} define a right-handed orthonormal coordinate system positioned at the satellite. Let r denote the distance of the satellite from the centre of the earth; thus $r\mathbf{u}$ is the vector from the centre of the earth to the satellite. All the variables listed in this paragraph are provided by the simulator.

Let \mathbf{x} denote a vector from the centre of the earth to the target. The vector

$$\mathbf{q} = \mathbf{x} - r\mathbf{u}$$

²The X , Y and Z axes referred to in this document are called the ‘spacecraft coordinate system axes’ in the L1B software interface specification for OCO.

points from the satellite to the target. Therefore, the satellite X -axis is defined by the unit vector

$$\mathbf{X} = -\mathbf{q}/q,$$

where q is the Euclidean length of \mathbf{q} . Because the satellite Z -axis is assumed to lie in the plane defined by \mathbf{u} and \mathbf{v} , we may represent it in the form

$$\mathbf{Z} = \alpha\mathbf{u} + \beta\mathbf{v},$$

where the scalars α and β must satisfy

$$\alpha^2 + \beta^2 = 1 \tag{1}$$

to ensure that \mathbf{Z} is a unit vector. Furthermore, because \mathbf{Z} must be orthogonal to \mathbf{X} ,

$$\mathbf{Z} \cdot \mathbf{X} = (\alpha\mathbf{u} + \beta\mathbf{v}) \cdot \mathbf{X} = 0,$$

which yields

$$\alpha\mathbf{u} \cdot \mathbf{X} = -\beta\mathbf{v} \cdot \mathbf{X}. \tag{2}$$

Using equation (1), we obtain

$$\alpha^2 = \frac{(\mathbf{v} \cdot \mathbf{X})^2}{(\mathbf{u} \cdot \mathbf{X})^2 + (\mathbf{v} \cdot \mathbf{X})^2} \quad \text{and} \quad \beta^2 = \frac{(\mathbf{u} \cdot \mathbf{X})^2}{(\mathbf{u} \cdot \mathbf{X})^2 + (\mathbf{v} \cdot \mathbf{X})^2}. \tag{3}$$

From the unit vectors \mathbf{X} and \mathbf{Z} , we define

$$\mathbf{Y} = \mathbf{Z} \times \mathbf{X}$$

to complete the orthonormal basis for the right-handed satellite coordinate system.

For the target to be visible from the satellite, the satellite must be above the tangent plane to the earth at the target. This requires that

$$\mathbf{u} \cdot \mathbf{X} > 0.$$

Furthermore, $\mathbf{v} \cdot \mathbf{X} < 0$ as the satellite approaches the target, while $\mathbf{v} \cdot \mathbf{X} > 0$ as it recedes from the target. Therefore, we require that $\beta > 0$ throughout the sequence of target mode observations, while α has the opposite sign to $\mathbf{v} \cdot \mathbf{X}$, as required by equation (2).

Let \mathbf{k} denote the local normal to the reference ellipsoid at the target \mathbf{x} . We need a unit vector \mathbf{p} perpendicular to \mathbf{X} that lies in the plane defined by \mathbf{X} and \mathbf{k} , as shown in figure 1. Such a vector may be written in the form

$$\mathbf{p} = \gamma\mathbf{k} + \delta\mathbf{X},$$

where

$$\gamma^2 + 2\gamma\delta\mathbf{k} \cdot \mathbf{X} + \delta^2 = 1. \tag{4}$$

Because this vector must be perpendicular to \mathbf{X} ,

$$\mathbf{p} \cdot \mathbf{X} = \gamma\mathbf{k} \cdot \mathbf{X} + \delta = 0,$$

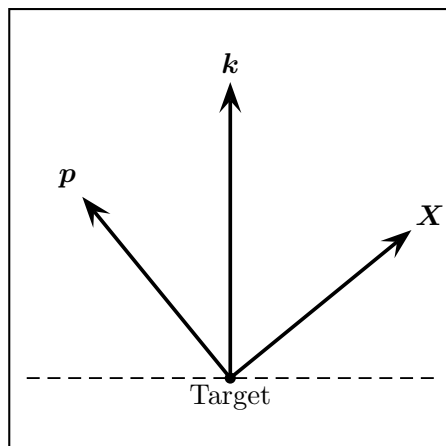


Figure 1: The unit vector \mathbf{X} points from the target to the satellite. The unit vector \mathbf{k} is the local normal at the target. The unit vector \mathbf{p} lies in the plane defined by \mathbf{X} and \mathbf{k} , and is perpendicular to \mathbf{X} . Furthermore, we require that $\mathbf{p} \cdot \mathbf{k} > 0$, as indicated in the figure.

from which it follows that

$$\delta = -\gamma \mathbf{k} \cdot \mathbf{X}. \quad (5)$$

Substituting δ from equation (5) into the normalization equation (4), we obtain

$$\gamma^2 = \frac{1}{1 - (\mathbf{k} \cdot \mathbf{X})^2} \quad \text{and} \quad \delta^2 = \frac{(\mathbf{k} \cdot \mathbf{X})^2}{1 - (\mathbf{k} \cdot \mathbf{X})^2}.$$

As indicated in figure 1, we require that

$$\mathbf{p} \cdot \mathbf{k} = \gamma(1 - (\mathbf{k} \cdot \mathbf{X})^2) > 0,$$

which requires

$$\gamma > 0.$$

The sign of δ then is determined via equation (5).

The plane defined by \mathbf{X} and \mathbf{k} (equivalently \mathbf{X} and \mathbf{p}) is the reference plane used in the calculation of Stokes' vector (I, Q, U, V) by the radiation code. However, OCO's polarizer transmits only radiation with its plane of polarization aligned with the Y -axis of the satellite. In order to calculate the power transmitted to the detector, we need to find Stokes' vector referred to the plane defined by \mathbf{X} and \mathbf{Y} , and to do this we need the angle ϕ defined in figure 2. Clearly,

$$\cos \phi = \mathbf{p} \cdot \mathbf{Y}.$$

The angle is positive if measured in a clockwise sense from \mathbf{p} to \mathbf{Y} . Thus, ϕ has the opposite sign to

$$\mathbf{X} \cdot (\mathbf{p} \times \mathbf{Y}).$$

Given that the orbit simulator provides the satellite position and velocity (respectively parallel to \mathbf{u} and \mathbf{t}) as well as the position of the target, it is a straightforward exercise to compute ϕ using elementary vector operations.

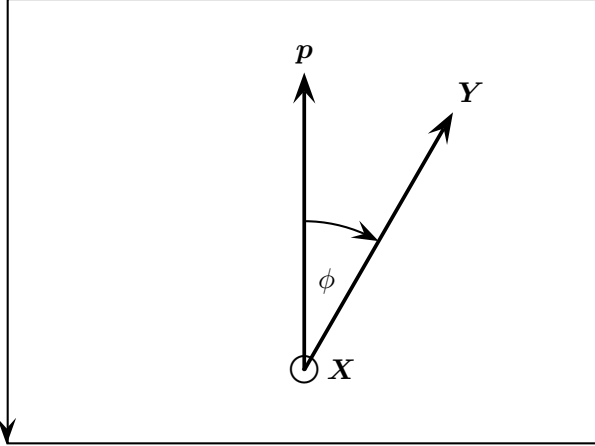


Figure 2: The circled dot denotes the point of an arrow heading out of the paper along the ray from the target to the satellite (the satellite X -axis). The vertical arrow \mathbf{p} denotes a unit vector perpendicular to \mathbf{X} in the plane defined by \mathbf{X} and the local normal at the target. Together with \mathbf{X} , \mathbf{p} defines the reference plane in which Stokes' vector (I, Q, U, V) is computed by the radiation code. The vector \mathbf{Y} denotes the satellite Y -axis, which also is perpendicular to \mathbf{X} . The angle ϕ is the angle between the planes defined by (\mathbf{X}, \mathbf{p}) and (\mathbf{X}, \mathbf{Y}) . The angle ϕ is positive if measured in the sense indicated by the arrow in the figure.

Measured intensity

Consider Stokes' vector in the form $(I_{\parallel}, I_{\perp}, U, V)$ when the reference plane is defined by \mathbf{X} and \mathbf{p} . Let $(I'_{\parallel}, I'_{\perp}, U', V')$ denote Stokes' vector referred to the plane defined by \mathbf{X} and \mathbf{Y} . Chandrasekhar (1950) proves that

$$\begin{pmatrix} I'_{\parallel} \\ I'_{\perp} \\ U' \\ V' \end{pmatrix} = \begin{pmatrix} \cos^2 \phi & \sin^2 \phi & \frac{1}{2} \sin 2\phi & 0 \\ \sin^2 \phi & \cos^2 \phi & -\frac{1}{2} \sin 2\phi & 0 \\ -\sin 2\phi & \sin 2\phi & \cos 2\phi & 0 \\ 0 & 0 & 0 & 1 \end{pmatrix} \begin{pmatrix} I_{\parallel} \\ I_{\perp} \\ U \\ V \end{pmatrix}.$$

The OCO polarizer accepts only the polarization parallel to the plane defined by \mathbf{X} and \mathbf{Y} , so the measured intensity is given by I'_{\parallel} ;

$$I'_{\parallel} = \cos^2 \phi I_{\parallel} + \sin^2 \phi I_{\perp} + \frac{1}{2} \sin 2\phi U. \quad (6)$$

Because

$$I = I_{\parallel} + I_{\perp} \quad \text{and} \quad Q = I_{\parallel} - I_{\perp},$$

equation (6) reduces to

$$I'_{\parallel} = \frac{1}{2}[I + \cos 2\phi Q + \sin 2\phi U]. \quad (7)$$

In the special case of measurements in the principal plane when $\phi = \pi/2$, the measured intensity reduces to

$$I'_{\parallel} = \frac{1}{2}[I - Q].$$

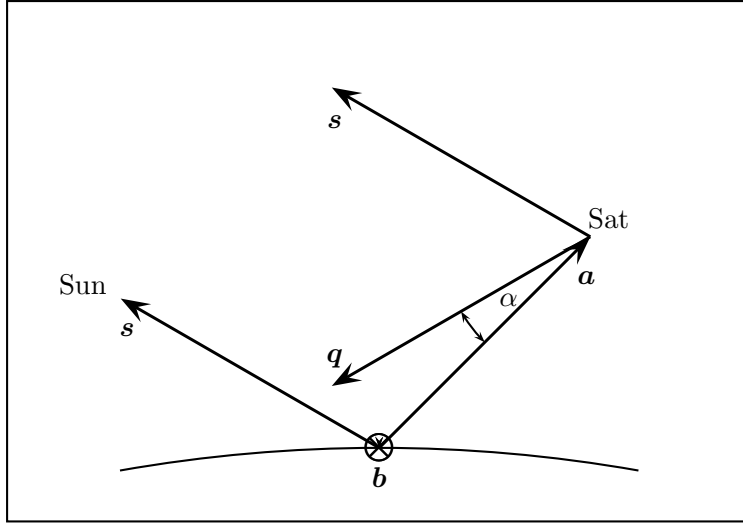


Figure 3: Vectors \mathbf{s} and \mathbf{a} point from the centre of the target area to the sun and satellite respectively. The vector \mathbf{b} (pointing into the paper) is parallel to the entrance slit. Vector \mathbf{q} points from the satellite to the centre of the misaligned target area. The vector \mathbf{q} is assumed to lie in the plane defined by \mathbf{s} and \mathbf{a} .

2.2 Slit misalignment and polarization angle

During characterization of the OCO spectrometers in the thermal vacuum chamber at JPL, it was found that the alignment of the spectrometers did not meet the design specifications. The cause was thought to be the release of tension in bolts securing the slit assembly of the weak CO₂ band spectrometer during thermal cycling of the instrument. While the O₂ A-band and strong CO₂ band slits remained closely aligned, the weak CO₂ band spectrometer slit suffered a parallel displacement that would cause approximately 300 m separation between the footprints on the ground in nadir mode. In order to assess the impact of this misalignment, the simulator was modified to allow arbitrary parallel displacements of all the spectrometer slits. The modifications required calculation for nadir, glint and target modes of the geometry and polarization angle for each sounding (footprint) within each frame, both with and without slit misalignment. The extra calculations are outlined in this subsection.

The area on the surface of the reference ellipsoid covered by the eight footprints of OCO is referred to as the target area, and the centre of this area as the target centre. Within the simulator, the slits of the three bands are assumed to be parallel but displaced laterally.

- (1) With reference to figure 3, let \mathbf{a} denote a unit vector from the target centre to the satellite. Ideally this unit vector will be parallel to the bore-sight axis of the instrument (the positive X -axis), but in practice it might not be so.
- (2) Let \mathbf{s} denote a unit vector from the target centre to the sun.
- (3) Let \mathbf{b} denote a unit vector parallel to the slit axis. In the simulator, it is assumed for

nadir and glint modes that \mathbf{b} is perpendicular to the plane defined by vectors \mathbf{s} and \mathbf{a} , and therefore is given by

$$\mathbf{b} = \frac{\mathbf{s} \times \mathbf{a}}{|\mathbf{s} \times \mathbf{a}|}.$$

- (4) Let \mathbf{c} complete the right-handed orthonormal coordinate system containing vectors \mathbf{a} and \mathbf{b} ,

$$\mathbf{c} = \mathbf{a} \times \mathbf{b}.$$

- (5) Again with reference to figure 3, let \mathbf{q} denote a unit vector that points from the satellite to the centre of the misaligned target area. The assumption of parallel displacement of the slit means that \mathbf{q} lies in the plane defined by \mathbf{a} and \mathbf{s} , and therefore may be represented in the form

$$\mathbf{q} = \sin \alpha \mathbf{c} - \cos \alpha \mathbf{a}.$$

Here α denotes the angular misalignment. Our present best estimates for α in the O₂ band, weak CO₂ band and strong CO₂ band are

$$\alpha = 0.0^\circ, \quad 0.0236^\circ \quad \text{and} \quad 0.0^\circ$$

respectively. These values would have been refined once OCO was in flight.

- (6) Let \mathbf{p}_n denote a unit vector pointing from the satellite to the centre of footprint n . We assume that \mathbf{p}_n lies in the plane defined by the slit axis \mathbf{b} and the vector \mathbf{q} that points to the centre of the misaligned target area. Thus

$$\mathbf{p}_n = \sin \beta_n \mathbf{b} + \cos \beta_n \mathbf{q},$$

where

$$\beta_n = (n - 4 - \frac{1}{2})\theta, \quad n = 1, 2, \dots, 8,$$

and 8θ is the angular width of the field of view along the slit axis. The value assumed in the simulator is $\theta = 0.1^\circ$. Hence,

$$\beta_1, \beta_2, \dots, \beta_8 = -3.5\theta, -2.5\theta, \dots, +3.5\theta.$$

- (7) Let \mathbf{t}_n denote a unit vector pointing from the centre of the earth to the centre of footprint n . Let \mathbf{k}_n denote the normal vector to the reference ellipsoid at \mathbf{t}_n .
- (8) The solar zenith angle θ_n at the the centre of footprint n is the angle between vectors \mathbf{s} and \mathbf{k}_n ,

$$\cos \theta_n = \mathbf{s} \cdot \mathbf{k}_n.$$

The solar azimuth φ_n is computed by projecting \mathbf{s} onto the tangent plane at \mathbf{t}_n , and then computing the angle between the projection and the vector pointing north.

- (9) The zenith angle θ'_n and azimuth φ'_n of the satellite are computed similarly using vector \mathbf{a} rather than \mathbf{s} .

- (10) The components of Stokes' vector reflected to the satellite are specified relative to the plane defined by the local normal vector \mathbf{k}_n at the centre of footprint n and the vector \mathbf{p}_n pointing from the satellite to the footprint. However, only photons with parallel polarization in the plane determined by vectors \mathbf{p}_n and the slit axis \mathbf{b} will be accepted by the polarizer, and hence contribute to the measured signal. Let ϕ_n denote the angle between these two planes, the reference plane for the radiative transfer and the plane of acceptance of the polarizer.
- (11) Let \mathbf{u}_n denote a unit vector perpendicular to the plane defined by \mathbf{p}_n and \mathbf{k}_n ,

$$\mathbf{u}_n = \frac{\mathbf{p}_n \times \mathbf{k}_n}{|\mathbf{p}_n \times \mathbf{k}_n|}.$$

Similarly, let \mathbf{v}_n denote a unit vector perpendicular to the plane defined by \mathbf{p}_n and the slit axis \mathbf{b} ,

$$\mathbf{v}_n = \frac{\mathbf{p}_n \times \mathbf{b}}{|\mathbf{p}_n \times \mathbf{b}|}.$$

The angle ϕ_n is the angle between vectors \mathbf{u}_n and \mathbf{v}_n , given by

$$\cos \phi_n = \mathbf{u}_n \cdot \mathbf{v}_n.$$

- (12) Again consider Stokes' vector in the form $(I_{\parallel}, I_{\perp}, U, V)$ when the reference plane is defined by \mathbf{p}_n and \mathbf{k}_n . Let $(I'_{\parallel}, I'_{\perp}, U', V')$ denote Stokes' vector referred to the plane defined by \mathbf{p}_n and \mathbf{b} . Chandrasekhar (1950) proves that

$$\begin{pmatrix} I'_{\parallel} \\ I'_{\perp} \\ U' \\ V' \end{pmatrix} = \begin{pmatrix} \cos^2 \phi_n & \sin^2 \phi_n & \frac{1}{2} \sin 2\phi_n & 0 \\ \sin^2 \phi_n & \cos^2 \phi_n & -\frac{1}{2} \sin 2\phi_n & 0 \\ -\sin 2\phi_n & \sin 2\phi_n & \cos 2\phi_n & 0 \\ 0 & 0 & 0 & 1 \end{pmatrix} \begin{pmatrix} I_{\parallel} \\ I_{\perp} \\ U \\ V \end{pmatrix}.$$

The OCO polarizer accepts only the polarization parallel to the plane defined by \mathbf{p}_n and \mathbf{b} , so the measured intensity is given by I'_{\parallel} ;

$$I'_{\parallel} = \cos^2 \phi_n I_{\parallel} + \sin^2 \phi_n I_{\perp} + \frac{1}{2} \sin 2\phi_n U,$$

which reduces to

$$I'_{\parallel} = \frac{1}{2}[I + \cos 2\phi_n Q + \sin 2\phi_n U]. \quad (8)$$

For the ideal case of observations in the principal plane, the polarization angle is 90° , but for the real instrument the polarization angle will vary with the footprint index from near 0° to near 180° in nadir mode.

3 Meteorology and trace gas profiles

The simulator provides two options for the meteorology.

The first calls upon a data base of representative ECMWF profiles prepared by Chevallier (2001). These have sixty layers, and the pressure levels are defined in terms of the surface pressure p_s by

$$p_n = a_n + b_n p_s, \quad n = 0, 1, \dots, 60.$$

At low levels the vertical structure is approximately a terrain-following σ -coordinate system, while at upper levels the b_n coefficients become small and the pressure levels are determined by a_n independently of the surface topography. The profiles in this data base are static, and their principal use in the simulator is for testing and training with a reproducible set of atmospheres. The static profiles were used to specify the profiles of pressure, temperature, specific humidity and the mixing ratios of cloud water and cloud ice.

A minor technical point concerns the calculation of the layer water and ice mass densities. Water and ice are specified in the ECMWF profiles as mass mixing ratios, and the pressure levels are determined uniquely by the surface pressure. Thus the layer water and ice mass densities also depend on the surface pressure. In order to avoid situations where varying the surface pressure also varied the amounts of cloud water and ice, the latter always were calculated with the surface pressure set to a reference value of one atmosphere.

The second option for the meteorology uses analyzed fields from ECMWF that are simultaneous and collocated with CloudSat profiles. In this case, the profiles of cloud water and cloud ice were derived from CloudSat on a vertical grid with 240 m spacing from the surface to the stratosphere. The corresponding profiles of pressure, temperature and specific humidity, interpolated to the CloudSat vertical grid and provided as part of the CloudSat data stream, were used for the meteorology in the simulator.

Because the CloudSat data stream provides meteorology only for the CloudSat vertical grid, which extends from the surface to approximately 20 km altitude, a simple stratosphere with three layers was imposed above the top of the CloudSat grid. The justification for using a simple model was that the weighting functions of the OCO retrieval algorithms roll off in the stratosphere, so inaccuracies of the temperature profile through the stratosphere should have only a minor effect upon the simulated spectra and the retrieved X_{CO_2} .

While the cloud and meteorology data provided by CloudSat are consistent and probably the best available representation of the real world complexity, they are available only for nadir mode. As a first approximation for glint mode, we simply assumed that the clouds and meteorology at the glint target would be identical to those at the subsatellite point, our intention being to replace this unrealistic approximation at a later stage. However, as so commonly happens, other priorities intervened and the initial ‘quick fix’ survives in the current version of the simulator. In one sense it doesn’t matter, because the purpose of the simulator is to calculate spectra with spatial scales of variability representative of the world OCO would observe. However, there are some glaring inconsistencies, the most notable being the surface height, which also is derived from the CloudSat data stream. Thus, when observing in glint mode over the ocean, the simulator will use the topography and meteorology for the subsatellite point, which sometimes causes oceans to appear at altitudes of several kilometres! Clearly this problem should be fixed.

The profiles of CO₂ volume mixing ratio (VMR) were derived from the Parameterized Chemical Transport Model (PCTM), driven by GEOS4 winds (Kawa et al., 2004). This data was generated on a 1.25° × 1.0° longitude-latitude spatial grid with a 450 s time step. It was provided on a vertical grid with 25 layers, whose pressure levels were defined in terms of the surface pressure in a manner similar to the ECMWF profiles. At each tick of the satellite clock, the profile of CO₂ VMR was interpolated in time and space to be simultaneous and collocated with the OCO target.

Because the PCTM data base is too large to hold in memory, a separate program, called `extract_pctm`, was written to read the PCTM data base and to interpolate the profiles of CO₂ VMR horizontally in space and in time to the footprints observed by the satellite. This process was performed for every tick of the satellite clock, producing a relatively small direct access file whose records were matched to the satellite footprints. The records come in pairs, one giving the pressure grid on which the CO₂ VMR is defined, and the other giving the profile of CO₂ VMR itself. Within the simulator, a second interpolation is performed to map the profile of CO₂ VMR from the PCTM vertical grid to the vertical grid used for the current footprint.

The program `extract_pctm` is under subversion control on the Colorado State University server `atlas.atmos.colostate.edu`. A copy may be checked out from the repository into a local directory (for example `pctm`) with the command

```
svn co svn+ssh://atlas.atmos.colostate.edu/data/OCO/repository/extract_pctm/ pctm
```

4 Cloud optical properties

The OCO simulator has two ways in which to provide the vertical distribution of cloud optical properties:

- (1) the ECMWF library (Chevallier, 2001);
- (2) the CloudSat 2B-CWC-RO product (Austin and Stephens, 2001; Austin, 2007).

Each approach provides the vertical profile of liquid (LWC) and ice (IWC) water content. In the case of ECMWF profiles, the vertical stratification consists of 60 layers, while for CloudSat a fixed vertical increment of 240 m is used from the surface to the stratosphere, typically giving more than 120 layers.

4.1 Liquid water cloud

To model cloud optical properties we assumed that the particle size distribution, $P(r)$, has the form of a gamma distribution,

$$P(r) \sim r^a \exp(-b r), \quad (9)$$

which depends on two parameters, one of which is determined by the LWC. To find the second parameter, we follow Bower et al. (1994) and use the correlation³ between the LWC

³Dimensional analysis of this equation shows that one of the numerical values is not dimensionless. Presumably the factor 100 is the combination of three separate factors: a factor 10⁶ in the denominator

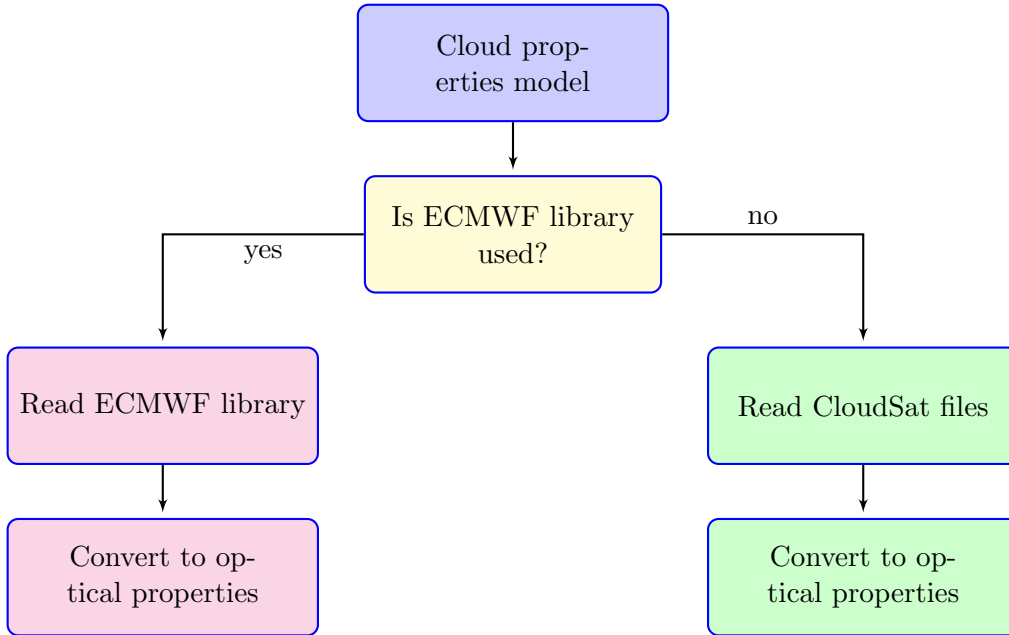


Figure 4: The decision diagram to calculate cloud optical properties.

and the effective radius, r_e ,

$$r_e = 100 \left(\frac{3 \text{LWC}}{4\pi N} \right)^{1/3}, \quad (10)$$

where LWC is expressed in units of gm^{-3} and

$$N = \begin{cases} 150 \text{ cm}^{-3} & \text{over ocean,} \\ 600 \text{ cm}^{-3} & \text{over land.} \end{cases}$$

Additionally, the effective radius is forced to be at least $4 \mu\text{m}$, and then it is rounded to the nearest integer below. The extinction and scattering efficiencies and phase matrix are precalculated using Mie theory with the code developed by Mishchenko (2000). The efficiencies and phase matrix moments for water drops are stored in files `wc_nnn.mie` and `wc_nnn.mom`, where `nnn` denotes the effective radius.

4.2 Ice water cloud

Following Ivanova et al. (2001), we assume that ice clouds consist of two fractions, large and small (subscripts l and s), and the particle size distribution has the form

$$N(r) = N_l(2r)^{v_l} \exp(-2\lambda_l r) + N_s(2r)^{v_s} \exp(-2\lambda_s r), \quad (11)$$

inside the parentheses representing the conversion of N from cm^{-3} to m^{-3} ; a second factor of 10^6 in the denominator representing the density of water in units gm^{-3} ; a factor 10^6 outside the parentheses representing a conversion from metres to micrometres.

Small mode	Large mode
$IWC_s = 1 - IWC_l$	$IWC_l = 0.89 - 0.89 \exp[-(r_{e,l}/25)^2]$
$v_s = 3.24$	$v_l = 2.64$
$\lambda_s = 365 \text{ cm}^{-1}$	$\lambda_l = (v_l + 1)/(2r_{e,l}) \text{ cm}^{-1}$
$r_{e,s} = 13 \mu\text{m}$	$r_{e,l} = 168.8 \exp(0.01754 T) \mu\text{m}$

Table 1: Parameters for Ivanova’s model. The total ice water content is normalized to unity. The temperature must be expressed in degrees Celsius.

where

$$N_x = IWC_x \frac{\lambda_l^{\beta_x + v_x + 1}}{\alpha_x \Gamma(\beta_x + v_x + 1)},$$

$x = l, s$, and the parameters are defined in table 1.

This model allows us to calculate for any layer the effective radius and number of particles. In a manner similar to that for liquid water cloud, the effective radius is forced to be a multiple of $5 \mu\text{m}$ lying between $10 \mu\text{m}$ and $90 \mu\text{m}$. The optical properties of ice cloud with a given effective radius are interpolated using the model published by Baum (2007) and Baum et al. (2005a,b). However, because the phase matrices for ice clouds are so strongly peaked in the forward direction, they were truncated at 10° , meaning that the phase matrix is constant for scattering angles less than 10° , and a δ -correction was applied to the extinction efficiency and single scattering albedo to compensate. The efficiencies and moments for ice crystals are stored in files `ic_nnn.mie` and `ic_nnn.mom`, where `nnn` denotes the effective radius of the large mode.

5 Aerosol optical properties

The OCO simulator offers two ways to include aerosol in atmospheric profiles.

5.1 Simple aerosol model

The first is a very simple proxy aerosol model, originally intended as a temporary first approximation. Aerosol is considered to be in three layers, 0–2 km, 2–5 km and 5–12 km. In the boundary layer 0–2 km, the aerosol is assumed to be either the oceanic or continental model (Shettle and Fenn, 1979) according to the surface type. In the range 2–12 km, continental aerosol is assumed. The option of a dust aerosol component between 2–5 km is included in the code to represent elevated dust clouds, such as Saharan dust, but presently is disabled. This model is a simplified version of the aerosol model suggested in Lenoble (1985). The efficiencies and moments for the simple aerosol model are stored in files `oceanic.mie`, `oceanic.mom`, `continental.mie` and `continental.mom`.

5.2 Calipso aerosol model

In this model, the vertical stratification of aerosol was constructed using the Calipso product `Calipso05kmALay`. Calipso provides a 2D profile (time and height) of the aerosol layer

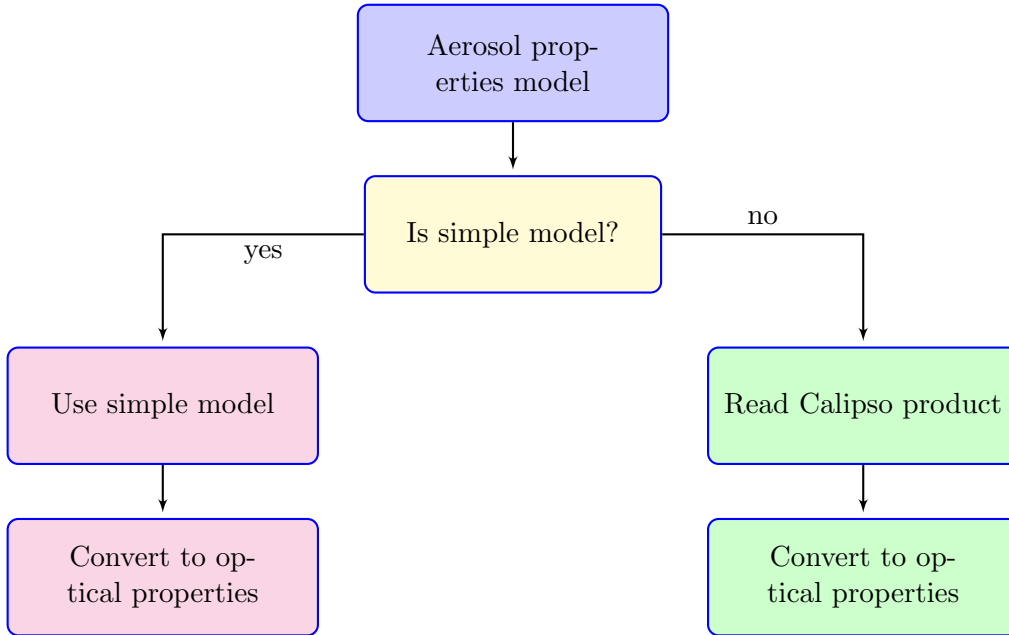


Figure 5: The decision diagram to calculate aerosol optical properties.

distribution (up to eight layers), including for each identified layer the heights of the top and bottom of the layer, the aerosol type and its optical thickness. As can be seen from figure 6, Calipso provides information for only about 25% of the frames. In order to populate the remainder of the frames with aerosol, the average aerosol profile was constructed for all orbits in the Calipso repeat cycle, 233 in number. This information is stored in files named `cal_summer_xxx.hdf`, where `xxx` denotes the orbit number, ranging from 001 to 233. The efficiencies and moments for Calipso aerosols are stored in files `clat_x.mie` and `clat_x.mom`.

5.3 Calipso aerosol models and their particle size distribution functions

Calipso uses models 1–6 of the eight listed in table 2. Because there is some uncertainty about the optical properties of the Calipso defined types, we substituted climatologically similar types from Shettle and Fenn (1979) and Dubovik et al. (2002).

In Dubovik et al. (2002) the particle size distribution has a bimodal lognormal functional form,

$$\frac{dV(r)}{d \ln r} = \sum_{i=s,c} \frac{C_{v,i}}{\sqrt{2\pi}\sigma_i} \exp \left[- \left(\ln \frac{r}{r_{m,i}} \right)^2 / (2\sigma_i^2) \right], \quad (12)$$

where $C_{v,i}$ denotes the particle volume concentration, measured in units $\mu\text{m}^3/\mu\text{m}^2$, $r_{m,i}$ is the modal radius, and σ_i is the standard deviation. The volume concentration C_v is related to the number concentration N_0 by

$$C_v = \frac{4\pi}{3} N_0 r_m^3 \exp[-9\sigma^2/2]. \quad (13)$$

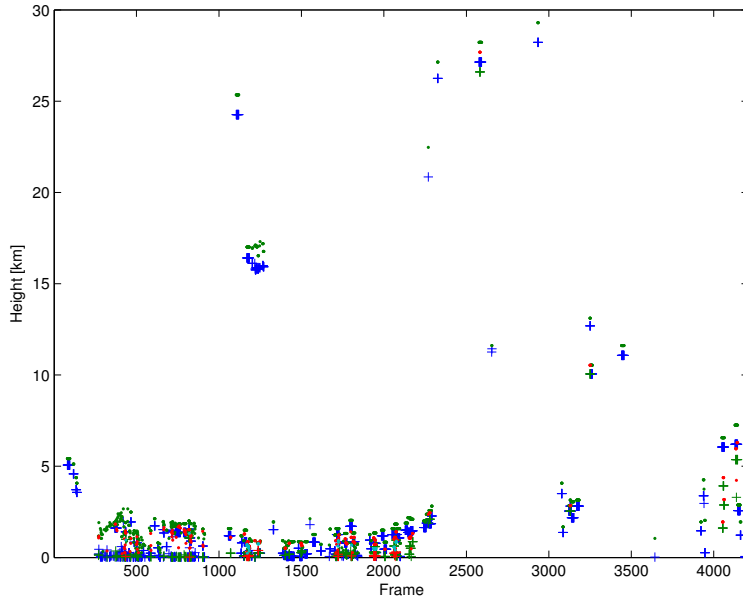


Figure 6: Density of aerosol profiles retrieved by Calipso. Pluses denote the layer bottoms, while dots denote the tops.

Calipso type	Name	Model substitution
0	not determined	none
1	clean marine	Shettle and Fenn (1979), oceanic
2	dust	Dubovik et al. (2002), Solar Village, Saudi Arabia, $\tau_{1020} = 0.5$
3	polluted continental	Dubovik et al. (2002), Maldives, INDOEX, $\tau_{440} = 0.8$
4	clean continental	Dubovik et al. (2002), GSFC, Greenbelt, MD, $\tau_{440} = 0.1$
5	polluted marine	Dubovik et al. (2002), Lanai, HI, $\tau_{1020} = 0.5$
6	smoke	Dubovik et al. (2002), South American Cerrado, Brazil, $\tau_{440} = 0.4$
7	other	none

Table 2: Substitutions for the Calipso aerosol types.

Parameter	Dust	Polluted continental	Clean continental	Polluted marine	Smoke
$C_{v,f}$	0.03	0.096	0.015	0.096	0.04
$r_{m,f}$	0.12	0.18	0.131	0.18	0.144
σ_f	0.4	0.46	0.38	0.46	0.47
$C_{v,c}$	0.47	0.12	0.014	0.12	0.052
$r_{m,c}$	2.32	3.11	3.08	3.11	3.474
σ_c	0.6	0.76	0.75	0.76	0.79
$n + ik$	$1.56 + i 0.001$	$1.44 + i 0.011$	$1.41 + i 0.003$	$1.44 + i 0.011$	$1.52 + i 0.015$

Table 3: Size distribution parameters and refractive indices for the aerosol models from Dubovik et al. (2002). The units of the concentrations $C_{v,f}$ and $C_{v,c}$ are $\mu\text{m}^3/\mu\text{m}^2$, while those of the modal radii $r_{m,f}$ and $r_{m,c}$ are μm . The subscripts f and c denote the fine and coarse modes of the bimodal size distributions.

A more common (from radiative transfer perspective) particle size distribution has the form

$$\frac{dN(r)}{d \ln r} = \sum_{i=s,c} \frac{N_{0,i}}{\sqrt{2\pi}\sigma_i} \exp \left[- \left(\ln \frac{r}{r_{g,i}} \right)^2 / (2\sigma_i^2) \right], \quad (14)$$

where

$$r_g = r_m \exp[-3\sigma^2]. \quad (15)$$

The parameters of the size distributions are listed in table 3. The clean marine model is from Shettle and Fenn (1979). It is the classic oceanic model. All the other models are from Dubovik et al. (2002), page 596. The dust model is the model for Solar Village, Saudi Arabia, with optical thickness $\tau_{1020} = 0.5$. The polluted continental model is the urban-industrial and mixed model for the Maldives, based on INDOEX data, and has $\tau_{440} = 0.8$. The clean continental model is the urban-industrial and mixed model for GSFC, Greenbelt, MD, with $\tau_{440} = 0.1$. The polluted marine model is the urban-industrial and mixed model for the Maldives, again based on INDOEX data, with $\tau_{440} = 0.8$. Finally, the smoke model is from observations of biomass burning for South American Cerrado, Brazil, with $\tau_{440} = 0.4$.

The optical properties of both the fine and the coarse fractions were calculated using a Mie code. The extinction efficiency factor, Q_{ext} , is represented in the form

$$Q_{ext} = \frac{\sum_{i=s,c} Q_{ext,i} N_{0,i} r_g^2}{\sum_{i=s,c} N_{0,i} r_g^2}, \quad (16)$$

with similar representations for the scattering efficiency factor,

$$Q_{sca} = \frac{\sum_{i=s,c} Q_{sca,i} N_{0,i} r_g^2}{\sum_{i=s,c} N_{0,i} r_g^2}, \quad (17)$$

and the coefficients of the decomposition of the phase matrix in Legendre series,

$$g_k = \frac{\sum_{i=s,c} g_{k,i} Q_{sca,i} N_{0,i} r_g^2}{\sum_{i=s,c} Q_{sca,i} N_{0,i} r_g^2}. \quad (18)$$

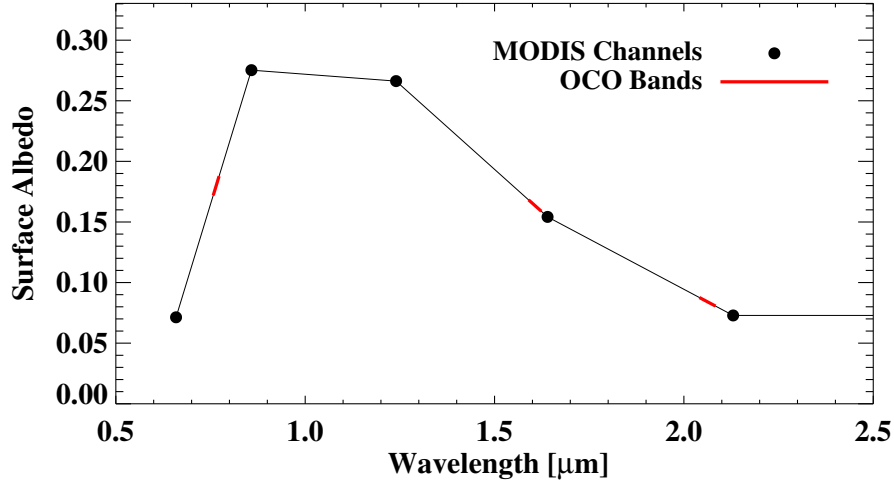


Figure 7: Sample albedo lookup from the MODIS channels to the three spectral regions spanned by the OCO bands. This sample is for the IGBP ‘mixed forest’ type.

6 Surface properties

The optical properties of the surface are modelled in the simulator as follows.

When the target is over land, there are two primary options. The first is a Lambertian surface whose albedo is drawn from a static MODIS albedo data base. The data base specifies albedo as a function of location on the globe, time of year and MODIS channel, and uses a $1/60^{\text{th}}$ degree grid. A linear interpolation is performed in frequency space to obtain albedos at the endpoints of each of the OCO bands. A sample of this process is shown in figure 7.

The second option over land enables a more realistic, non-Lambertian BRDF. However, because there is no global data base of fully polarized BRDFs available for the OCO spectral bands, these BRDFs are synthesized as follows. First, a scalar BRDF is estimated from the MODIS sixteen-day BRDF product MCD43B1. This product contains coefficients for three kernels, the first representing isotropic reflection and the other two linearized approximations to the Ross-thick and Li-sparse kernels (Wanner et al., 1997; Li and Strahler, 1992). These coefficients are provided for each of seven MODIS ‘land bands’, which subsequently are interpolated to the endpoints of the OCO bands. However, this is a purely scalar BRDF and provides no information on the surface polarization characteristics. The latter are estimated using a simple model based on POLDER observations (Breon, 2008), which are aggregated into a polarized BRDF for each of sixteen IGBP land surface types. This model was derived specifically for the POLDER 550 nm frequency, and is used directly; no frequency interpolation is performed, and thus the polarization characteristics are independent of frequency. Thus, in the 4×4 polarized BRDF matrix, which describes how each Stokes’ parameter is reflected by the surface into each of the four possible Stokes’ parameters, the $I \rightarrow I$ pathway is taken from the frequency-dependent MODIS (MCD43B1) three-kernel

model, and the remaining fifteen components are taken from the frequency-independent POLDER model. While this model is an approximation, it nonetheless should provide reasonably realistic surface BRDFs.

Over ocean, a fully-polarized Cox and Munk (1954a,b) surface plus a foam component is employed. The Cox-Munk surface includes a gaussian distribution of planar facets, each described by its Fresnel reflection coefficient; the resulting BRDF is primarily dependent on the wind speed and the refractive index of the water. The wind speed was taken from the ECMWF forecast, while the refractive index was taken from published tabulations as a function of wavelength (Palmer and Williams, 1974). The foam component assumes a fractional foam coverage using the parameterization of Monahan and ÓMuircheartaigh (1980); the albedo of the foam was derived from the model of Whitlock et al. (1982) with the modification by Koepke (1984), which takes into account the impact of foam age on albedo as well as other effects. The foam BRDF therefore is purely Lambertian, while the Cox-Munk BRDF is fully polarized. The two BRDFs are combined according the fraction of the ocean surface covered with foam, as determined by the wind speed.

7 Radiative transfer

Once the physical properties (temperature, pressure, water vapour, etc), surface properties and aerosol optical properties have been specified, the profile is passed to the radiative transfer module to calculate spectra in the OCO bands. The steps in this process are as follows:

- (1) compute gas absorption optical depths;
- (2) compute Rayleigh scattering;
- (3) combine gas, Rayleigh, and aerosol optical properties;
- (4) compute surface BRDF at band endpoints;
- (5) compute high-resolution reflectance spectrum;
- (6) multiply by solar spectrum;
- (7) Doppler shift resulting spectrum into OCO rest frame;
- (8) convolve with instrument response.

7.1 Spectroscopy and gas absorption

In the OCO bands, the gas absorption cross sections are taken from an absorption coefficient (ABSCO) database, which is a synthesis of HITRAN 2004 (Rothman et al., 2005) with CO₂ line updates from 4300–7000 cm⁻¹ based on the work of Toth et al. (2008). The spacing of the high-resolution grid is 0.01 cm⁻¹, which resolves individual O₂ and CO₂ lines in the near infrared with a minimum of two points per Doppler width (Bösch et al., 2006); calculations show that this introduces errors no larger than 0.08% in the strong CO₂ band, with somewhat smaller errors in the other bands. Only O₂ absorption is considered in the

O₂ A-band, while both CO₂ and H₂O absorption are considered in the weak and strong CO₂ bands. Absorption by all other gases is small in these bands, and presently is ignored by the simulator. Overlap of the Chappuis band of O₃ with the O₂ A-band will be added at a later date.

7.2 Rayleigh scattering

Rayleigh scattering is accounted for in all OCO bands, though it is most important in the O₂ A-band. The Rayleigh scattering cross section is calculated using the classic model (for example van de Hulst, 1957),

$$\tau_r = \frac{24\pi^3 (n_s^2 - 1)^2 6 + 3\rho}{N_s^2 \lambda^4 (n_s^2 + 2)^2 6 - 7\rho}, \quad (19)$$

where N_s is the molecular number density of air and n_s is its index of refraction, both evaluated at the same pressure and temperature. According to Lorentz-Lorenz theory, the product of the two factors in equation (19) involving N_s and n_s is independent of pressure and temperature. We take $N_s = 2.546899 \times 10^{19}$ molecules/cm⁻³ at 288.15 K and 1013.25 hPa, as suggested by Bodhaine et al. (1999). The index of refraction for air at standard pressure and temperature is taken from the four-parameter fit by Peck and Reeder (1972); this was for a CO₂ concentration of 300 ppmv, but the effect on the result is small (less than 0.01%), so the error was deemed acceptable. The symbol ρ denotes the depolarization factor, which is taken to be a constant within each OCO band. The depolarization factors for the OCO bands were calculated according to the scheme of Bodhaine et al. (1999), considering the presence of N₂, O₂, Ar and CO₂. A CO₂ concentration of 385 ppmv was assumed. The resulting depolarization factors were 0.02771, 0.02726 and 0.02721 for the O₂ A-band, weak CO₂ band and strong CO₂ band, respectively. The Rayleigh phase matrix, including polarization, is a standard formulation (for example Hansen and Travis, 1974).

The Rayleigh optical depth of an atmospheric layer is the product of the cross section in m² per molecule and the total number of molecules per m² in the layer, $N_{tot}\Delta z$. Using the hydrostatic equation, it can be shown that this quantity is given by

$$N_{tot}\Delta z = \frac{N_A \Delta P}{M_{dry} g} \left(1 + \frac{1 - \epsilon}{\epsilon} q \right), \quad (20)$$

where ΔP is the pressure width of the layer in Pa, N_A is Avogadro's number, M_{dry} is the molar mass of dry air (28.96×10^{-3} kg/mol), g is the mean gravitation acceleration in the layer in units m/s², q is the layer-mean specific humidity in kg/kg, and $\epsilon = 0.622$ is the ratio of the molar mass of water vapour to that of dry air.

7.3 Composite atmospheric optical properties

At this point the absorption and scattering coefficients due to gas absorption, Rayleigh scattering and both absorption and scattering by clouds and aerosols are combined on the 0.01 cm⁻¹ grid used for gas absorption. Because the scattering characteristics vary so slowly over the band, only the optical depth and single scattering albedo are calculated

at each high resolution spectral point; the phase matrices (combining Rayleigh, cloud and aerosol) are calculated only at the band endpoints, and later are interpolated linearly to the high resolution spectral grid.

7.4 Surface optical properties

As with aerosol, the surface BRDF is calculated only at the band endpoints, and is interpolated linearly in between. An interpolation is needed because the parameters that determine the BRDF, such as the index of refraction for ocean and the MODIS BRDF parameters for land, vary spectrally. The BRDF represents the effect upon Stokes' vector of reflection from one quadrature angle into another. As will be explained below, two sets of quadrature angles are used, corresponding to a low number of streams (typically 6) and a high number of streams (typically 24). The values and ordering of the quadrature angles are chosen to match precisely those used by the monochromatic radiative transfer.

7.5 High-resolution radiative transfer

Once the optical properties of the atmosphere and surface have been specified, radiative transfer calculations are performed on a 0.01 cm^{-1} spacing grid. Because OCO would have been sensitive to polarization, Stokes' I , Q and U must be calculated. It is not necessary to calculate Stokes' V for two reasons: typically the atmosphere and surface do not generate circular polarization; and OCO is not sensitive to circularly polarized radiation. In order to estimate I , Q and U at the top of the atmosphere (TOA) for each high-resolution spectral point, a three-step approach is taken:

1OS — calculate the exact first-order of scattering result for I , Q and U ;

I_{ms} — calculate the multiply-scattered TOA radiance for I ;

2OS — calculate the second-order of scattering contributions to Q and U , as well as the polarization correction for the second order of scattering to I .

Here we have named the three radiative transfer subprocesses 1OS, I_{ms} and 2OS. By combining the results of these individual calculations, the TOA radiance can be estimated reasonably accurately for nearly clear scenes (Natraj et al., 2007).

The three terms in the list above are calculated by separate codes. Both the 1OS and 2OS terms are part of the 2OS suite of codes described in Natraj et al. (2007). Note that I_1 is calculated using the TMS correction of Nakajima and Tanaka (1988), and all three first-order scattering terms include the direct beam scattered from the surface. The term I_{ms} is the multiply-scattered intensity term, and is calculated using the Successive Orders of Interaction (SOI) radiative transfer model (Heidinger et al., 2006) with slight updates for the near infrared. The SOI model employs the delta-M phase-function truncation technique of Wiscombe (1977). The SOI model is both fast and accurate (O'Dell et al., 2006).

7.6 Low-streams interpolator

In terms of overall computational burden, the 1OS calculation is extremely fast in comparison to the SOI and 2OS calculations. When run with sufficient angular resolution, the

latter codes are much too slow to calculate the tens of thousands of high resolution radiances required for a brute-force approach. A faster alternative is described below.

Both the SOI radiative transfer model and the 2OS model rely on a quadrature-based approach, wherein the code only treats radiation coming from specific, discrete zenith angles or ‘streams’, and interpolates between these angles to find the radiation at an arbitrary angle. In the nomenclature, a code is said to be run with a total of N streams, where $N/2$ is the number of streams in either the upper or lower hemisphere. The computational burden in theory is $O(N^3)$, because the codes largely rely on multiplication and inversion of $N \times N$ matrices. However, often there is significant overhead, which lessens the extreme dependence on N to be more like $O(N^2)$, especially for lower numbers of streams.

The number of streams and vertical layers required to achieve a given accuracy depends on the atmosphere. Generally, the stronger the scattering, the more streams required. However, tests at CSU have shown that a minimum of eight streams usually is required, and up to twenty-four streams would be highly desirable for the OCO retrieval code. Unfortunately, twenty-four streams are much too costly to calculate the radiance for every high resolution spectral point.

Additionally, the simulator often is run with a large number of vertical layers, which further adds to the computational cost of a single monochromatic radiance calculation. The cost of calculating optical properties at a fine vertical resolution is small in comparison with the cost of calculating the multiply scattered radiance. Similar to the number of streams question, there is the additional question of how many vertical layers are required by the radiative transfer. For instance, given the composite optical properties of each layer at a given vertical resolution, potentially we could combine the optical properties of two similar, adjacent layers into a single layer as follows:

$$\begin{aligned}\tau &= \tau_1 + \tau_2, \\ \varpi &= \frac{\varpi_1 \tau_1 + \varpi_2 \tau_2}{\tau}, \\ P_l &= \frac{P_{l,1} \varpi_1 \tau_1 + P_{l,2} \varpi_2 \tau_2}{\varpi \tau},\end{aligned}$$

where indices 1 and 2 represent the original layers to be combined, and the quantities on the left represent the optical properties of the combined layer. Within the radiative transfer module, there is an option that allows every N_{sum} set of layers to be combined into a single layer. For instance, if the original number of vertical layers is 60 and $N_{sum} = 3$, the resulting number of vertical layers would be 20. In principle we can specify N_{sum} separately for each radiative transfer subprocess (1OS, I_{ms} and 2OS).

Physically, this high vertical resolution is only required in the presence of cloud or aerosol layers. Gas absorption and Rayleigh scattering both vary smoothly in the vertical, and thus do not require particularly high vertical resolution. Thus, similar to the number of streams, it is atmospheric scattering that drives the number of vertical layers.

The preceding discussion demonstrates that scattering drives the computational cost of monochromatic radiance calculations. Fortunately, we can exploit the fact that the scattering characteristics of clouds, aerosols and the surface vary much more slowly than the gas absorption coefficients within the narrow OCO bands. Indeed, high spectral resolution is only required because of the gas absorption. Conversely, individually slow radiance calculations are only required by atmospheric scattering. A method, called the ‘low-streams

Calculation Type	1OS	I_{ms}	2OS
Low accuracy	Exact $N_{sum}=1$	6 streams $N_{sum}=3-5$	None
High accuracy	Exact $N_{sum}=1$	24 streams $N_{sum}=1$	24 streams $N_{sum}=1$

Table 4: Typical settings for low and high-accuracy calculations for the LSI technique.

interpolator’, has been developed to decouple these effects to speed up the radiative transfer dramatically. Below is a brief summary of this technique; the interested reader should see O’Dell (2009) for more details.

The basic idea of the low-streams interpolator is to perform a low-accuracy calculation of Stokes’ parameters I , Q and U at each high-resolution spectral point, and then to correct these computations using the results of a small number of high-accuracy calculations. If the errors are primarily from scattering processes, and these processes vary smoothly across the band, the errors may be parameterized in a simple way.

Table 4 shows the two types of monochromatic radiance calculations we will be doing. ‘High accuracy’ is meant to be our best estimate of the radiance, while ‘low accuracy’ is meant to be fast, with errors only from scattering and not absorption processes. Both perform identical first-order of scattering (1OS) calculations, exact and at the highest available vertical resolution. This is acceptable because this calculation is extremely fast. Both perform a scalar, multiple-scattering calculation, but the low-accuracy calculation uses six streams and N_{sum} is typically between three and five, while the high-accuracy calculation uses twenty-four streams and $N_{sum} = 1$. Because the cost of the multiple-scattering calculation with N streams and L layers is $O(LN^3)$, we could expect the low-accuracy I_{ms} calculation to be as much as 320 times faster than the high-accuracy I_{ms} calculation! Finally, because multiply-scattered polarized radiation typically is much smaller than the other contributions to the radiance, we simply neglect Q_2 and U_2 in the low-accuracy calculation.

With these conventions in mind, the following list describes the LSI recipe.

- (1) Within each OCO band, perform a low-accuracy calculation of Stokes’ parameters I , Q and U at each spectral point. In the O_2 A-band, for example, more than 20,000 monochromatic radiance calculations are required.
- (2) Form average optical properties for all spectral points with similar total gas optical depths. Create approximately twenty logarithmically-spaced bins in the vertically-integrated gas absorption optical depth.
- (3) Perform low and high-accuracy radiance calculations for the optical properties in these bins. Take the phase function and surface properties to be equal to those at the band center.
- (4) For each bin, determine the errors in the low-accuracy calculations of I , Q and U , relative to the high-accuracy calculations.

- (5) Assume that the error varies linearly in total gas optical depth, and approximate the error of the low-accuracy calculation relative to the high-accuracy calculation by interpolation for each high-resolution spectral point.
- (6) Correct the low-accuracy calculations using these error estimates. For Stokes' I , use relative errors, while for Stokes' Q and U use absolute errors.

Implicit in this technique is the assumption that the errors incurred with only six streams vary smoothly as functions of the logarithm of the total column optical depth. Fortunately such is the case, as is shown by O'Dell (2009). The errors for I , Q and U always vary relatively smoothly with total gas optical depth, and this is especially true for the multiple-scattering components, which we care about in this case. There is some scatter for unknown reasons, but this typically is small and leads to an acceptable error once the radiances have been convolved with the ILS. The result is that virtually all the time is spent on the 20,000 or so low-accuracy calculations; the approximately twenty high-accuracy calculations take significantly less time, along with the error interpolation required to correct the low-accuracy calculations. This drastically improves the speed of the overall calculation; factors of tens to thousands are possible, depending on the number of streams desired.

7.7 Detection by the instrument

The measured spectrum is obtained by convolving the high-resolution radiances with the line shape function of the instrument. This is a three-step process. First, the calculated Stokes' parameters are combined to form the single linear polarization detected by the instrument,

$$I_{meas} = \frac{I + Q \cos 2\phi + U \sin 2\phi}{2}, \quad (21)$$

where ϕ is the instrument polarization angle. For both nadir and glint modes, $\phi = 90^\circ$, in which case OCO would be insensitive to U , but in target mode OCO would be sensitive to all three Stokes' parameters.⁴

After the polarization has been accounted for, I_{meas} is multiplied by the solar spectrum. The solar model employs an empirical list of solar line parameters as well as a model for the solar continuum; see Bösch et al. (2006) for further details. The solar spectrum must be Doppler-shifted, so it is the spectrum as seen in the rest frame of the target on the earth. The resulting high-resolution spectrum subsequently is Doppler-shifted into the rest frame of the moving observatory. Both the sun-earth and earth-observatory Doppler velocities are calculated by the orbital model.

Finally, the Doppler-shifted, high-resolution spectrum is convolved with the line shape function of the instrument to simulate the measured spectrum. The simulator uses the measured ILS of the now-defunct OCO. A sample ILS is shown in figure 8.

⁴In practice, the polarization angle deviates from 90° , varying from footprint to footprint, and depending partly upon the degree of slit misalignment.

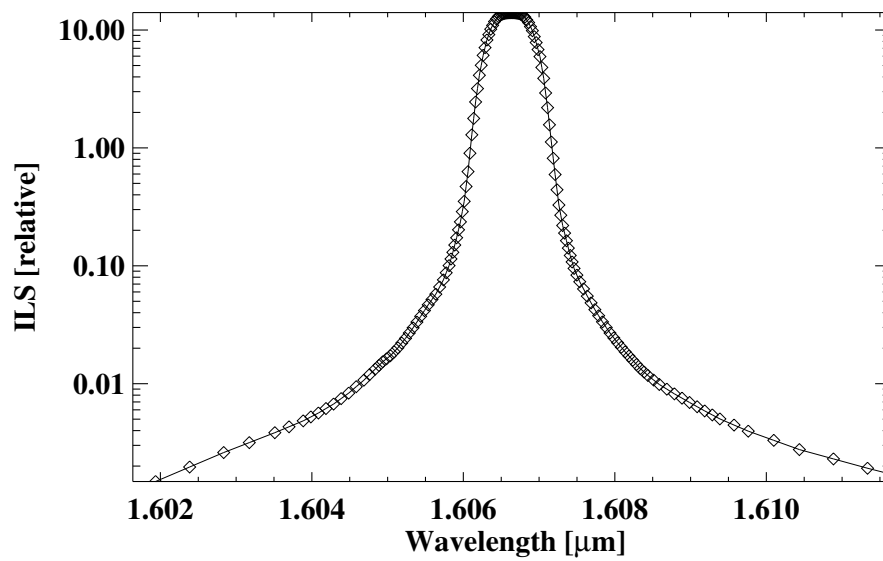


Figure 8: Sample instrument line shape function, as measured on the OCO instrument during thermal vacuum tests at JPL. This particular line shape is near the weak CO_2 band center for footprint 5.

8 Using the simulator

The steps below outline the process. The input files are described in more detail in the following subsections.

- (1) The simulator code is located on server `atlas.atmos.colostate.edu`, where it is under subversion control. A copy may be checked out from the repository into directory `sim` (for example) with the subversion command

```
svn co svn+ssh://atlas.atmos.colostate.edu/data/OCO/repos/oco/trunk/orbit sim
```

- (2) Immediately after checking out the simulator from the repository, make a copy of `dat_local`; for definiteness in this description, it will be assumed that the copy is called `dat_customized`.

- (3) Change to the `src` subdirectory, and set environment variables with the command

```
source setup.tcsh
```

for a tcsh shell, or

```
source setup.sh
```

for a bash shell.

- (4) Make the program in the `src` subdirectory with the command

```
make all
```

The orbit simulator can also operation on an MPI-based distributed memory cluster by processing different frames and soundings on different nodes in parallel to speed up operation. To compile the program for MPI-based operation, use the command

```
make MPI=t all
```

- (5) Execute the program in the `src` subdirectory with the command

```
./orbit ../dat_customize/
```

if interactive editing of the input data is required, and

```
./orbit ../dat_customize/ !
```

otherwise. Note the trailing `/` after `dat_customize!` The menus have two fields, a message field on the left-hand side that is fifty characters wide, and a value field on the right that also is fifty characters wide. When a menu is displayed on the screen, the user can move about the value field with the arrow and ENTER keys, over-typing the default values as required. Once the desired values have been set, the menu may be accepted with the key chord control-D. The modified menu will be written to the log file, creating a record of the selected options. If the menus are suppressed, then the default values in the menus will be used by the program.

The orbit simulator does not support interactive editing of menus when running in MPI mode. To run in MPI mode, use the `mpirun` command as follows

```
mpirun ./orbit ../dat_customized/ !
```

The `mpirun` command on `ococluster.cira.colostate.edu` is a version modified from the MPICH MPI implementation that automatically submits the job to the Torque/PBS batch scheduling system using all processors. The program will start when enough processors are available to run it.

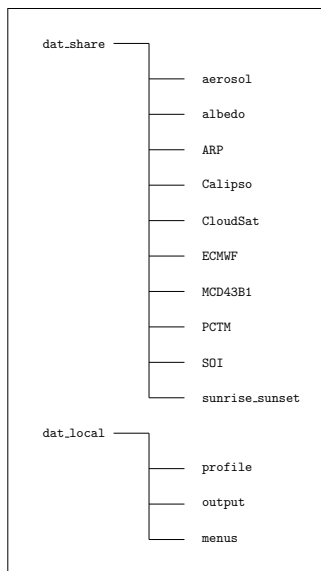


Figure 9: Structure assumed for the data directories.

- (6) In addition to parallelization via MPI, the subversion repository includes a script (called `launch_orbit`) to run multiple instances of the orbit simulator on different machines. Instructions for using `launch_orbit` are in section 8.3.

8.1 Shared input data in `dat_share`

The structure assumed for the input data directory is as shown in figure 9. There are two primary directories, `dat_share` and `dat_local`. The top-level directory `dat_share` contains collections of data likely to be used by many users, and therefore is best shared as it is voluminous and time consuming to download. The contents of its subdirectories are as follows.

`albedo`

Subdirectory `albedo` contains the default scalar albedo data base derived from MODIS. The data base has two components, the first being a large file listing for each target an integer defining the International Geosphere-Biosphere Project (IGBP) classification of the target. The second is a set of default albedos associated with the different target classes. The default albedos are defined within `AN_Albedo_Module`.

The MODIS albedo data base has albedos as a function of location on the globe, time of year, and MODIS channel. A linear interpolation is performed within `AN_Albedo_Module` in order to obtain albedos at the OCO bands; albedo slopes within the band are also obtained during this interpolation process. This process is described in more detail in section 6.

aerosol

Subdirectory `albedo` contains files that define the phase matrices of the different aerosol types. Files with extension `.mie` specify the extinction efficiency, scattering efficiency and single scattering albedo at the six wavelengths defining the limits of the three OCO bands. Files with extension `.mom` contain the moments of the phase matrices for each of the six wavelengths. For each wavelength and each moment index, there are six components of the phase matrix defined in the Siewert convention.

Files with names `wc_nnn.mie` and `wc_nnn.mom` are for water clouds containing drops with effective radius `nnn`, expressed in μm . Similarly, files `ic_nnn.mie` and `ic_nnn.mom` are for ice clouds with effective radius `nnn`. Generally, aerosol type `name` will have files `name.mie` and `name.mom`.

SOI

The acronym SOI stands for Successive Orders of Interaction, which is the name of the technique used by the simulator to solve the radiative transfer equation. Subdirectory `SOI` contains many data files needed by the radiative transfer, as listed below.

Gas absorption lookup tables. These files contain the absorption cross-sections of the gases in the OCO bands. The file names typically have the form `gasabs_abcscT14_b.dat`, where `b`, taking values 1, 2 and 3, is the OCO band. There are different sets of files depending on which spectroscopy is used. These files are in a binary format particular to the simulator.

Solar lines file. This is an ASCII file that contains the details of the solar lines included in the simulator. The standard file is `solar.h92`.

Optimal sampling files. These files are used to accelerate the radiance calculations by optimally sampling the high-resolution spectral points. There are different sets, depending on which gas lookup tables are used. Also, typically there is a standard set and a conservative set, where the latter has somewhat lower errors at the expense of longer calculations. The typical set to use is `optimal_sampling_ABSCO_conservative_b.dat`, where again `b` is the OCO band number.

Low-streams interpolator files. These are small ASCII files that define the binning scheme used by the low-streams interpolator module, part of the radiative transfer. There is one per OCO band, named `lsi_bounds_b.txt`, where again `b` is the OCO band number.

Instrument dispersion file. This ASCII file defines the spectral dispersion of the OCO instrument.

Instrument line shape (ILS) file. This is binary file that defines the instrument line shape function (ILS) for each pixel in each band of the OCO instrument. The file that matches the OCO L1B definition is `ils_tables_6816_L1B_1016pixels.dat`.

PCTM

Subdirectory PCTM contains two types of files, the first being global fields of CO₂ volume mixing ratio (VMR) predicted by the PCTM (Kawa et al., 2004), and the second being subsets extracted along specific orbit tracks.

The present version contains only PCTM.288x181x25_co2_sep14_30.gra, which specifies the CO₂ VMR on a 1.25° longitude grid, a 1° latitude grid and a vertical grid with 25 layers. The data is for the sixteen-day period from September 14–30, 2006. The CO₂ profiles were generated at 7.5 min (450 s) time increments. Simulations for other periods will require new PCTM runs, which can be performed at CSU on request.

The present directory also contains files with names 20060914_nnn_M.CO2.dat, which contain subsets extracted from the PCTM file above for orbit *nnn* and scan mode *M*, where the latter may denote *N*, *G* or *T* for nadir, glint and target modes. Usually, the target mode files also will have the name of the target (such as Darwin or Bremen) appended to the file. Subsets are extracted with the utility called `extract_pctm`, which was introduced in section 3.

Each of the subset orbit files contains *inter alia* a header record that lists the starting time of the orbit and the time increment between samples. When the simulator is started, the header record is checked for consistency with other data. If a mismatch is found, the user is given the opportunity to proceed anyway, a feature that often is useful when testing. However, for final production runs, the orbit parameters specified in the header of the subset file should match those specified in the orbit menu (described later).

MCD43B1

The acronym MCD43B1 denotes the combined Terra and Aqua MODIS BRDF produced for land targets every sixteen days with nominal 1 km spatial resolution. The product contains coefficients for three kernels, the first representing isotropic reflection and the other two linearized approximations to the Ross-thick and Li-sparse kernels (Wanner et al., 1997; Li and Strahler, 1992). The files in the present directory are for the sixteen-day period from September 14–30, 2006. For other periods, the user must download the relevant files from the MODIS repository.⁵

Each sixteen-day cycle covers the entire globe with about 450 tiles, whose names have the form

MCD43B1.Ayyyyddd.hxx.vyy.rrr.yyydddhhmmss.hdf.

The first *yyyy* and *ddd* refer to the year and day of the year at the start of the sixteen-day period. The tiles are labelled by a horizontal index *xx* and a vertical index *yy*. The tag *rrr* is the release number. The final *yyyydddhhmmss* is the year, day, hour, minute and second at which the file was produced. The simulator calculates the tile coordinates from the satellite position and the scan mode, and therefore is able to synthesize the MODIS file name, except for the date and time of production, which generally are unpredictable. Therefore, a symbolic link must be made to every MODIS file, removing the release number, date and time of production:

⁵The code can use either release 4 or release 5 files. The module `modis_hdf_module` contains a parameter called `Release` whose value will select between the two. However, the user must set this parameter manually.

```
ln -s MCD43B1.Ayyyyddd.hxx.vyy.rrr.yyyydddhhmmss.hdf MCD43B1.Ayyyyddd.hxx.vyy.hdf
```

The simulator will search for the symbolic links.

CloudSat

The CloudSat data is contained in files with the names

```
yyyydddhhmmss_nnnn_CS_ECMWF_AUX_GRANULE_P_R04_E_02.hdf
```

and

```
yyyydddhhmmss_nnnn_CS_2B_CWC_RO_GRANULE_P_R04_E_02.hdf .
```

Here `yyyy`, `ddd`, `hh`, `mm` and `ss` are the year, day of the year, hour, minute and second at the start of the granule. Each granule contains a full orbit, commencing with the south-bound equator crossing. The number `nnnn` is the orbit number. The ECMWF data has been interpolated in time and space (both horizontally and vertically) to the CloudSat grid. Finally, `CWC_RO` stands for ‘cloud water content, radar only’.

The shared data directory presently contains data for only a few orbits, starting on September 14, 2006. The user must locate and download the CloudSat data for other periods.

In addition to the `hdf` files, an indexing file called `timefile.dat` is needed. For each orbit, it lists the starting time (in seconds since midnight UT on 1993-01-01) and the component `yyyydddhhmmss_nnnn_CS_` of the corresponding file name.

8.2 Customized input data in `dat_local`

When a copy of simulator is checked out from the repository, a top-level directory `dat_local` containing templates of customizable input files will be created. The user immediately should make a copy of `dat_local`; for definiteness in this description, it will be assumed that the copy is called `dat_customized`. The contents of the subdirectories of `dat_customized` are as follows.

`profile`

Subdirectory `profile` is intended for output. It will contain ASCII files of spectra, written by the SOI code. Its principal use is in debugging and testing.

`output`

Subdirectory `output` also is intended for output. If the file menu (described below) specifies that the root of the output file is (for example) `test`, then the simulator will place in subdirectory `output` the following files:

`test.hdf`, the L1B file with simulated spectra and other meta-data;

`test.log`, an ASCII log file listing over thirty parameters that characterize the profiles processed;

```

# FILES MENU
# *****
#
# Shared data path                './dat_share/'
#   ARP file name                 'ARP/oco_ArpND_00333_00444_080822173456.hdf'
#   CO2 file name                 'PCTM/20060914_008_N_CO2.dat'
#   'PCTM/20060914_008_N_CO2.dat'
#   'PCTM/20060914_008_G_CO2.dat'
#   'PCTM/20060914_001_T_CO2_Bremen.dat'
#   Default albedo file name      'albedo/scene_type.dat'
#   SOI endpoints file name       'endpoints.oco'
#   SOI dispersion file name      'dispersion_start_1.oco'
#   SOI prefix for gas abs files  'gasabs_abscoT14_oco_'
#   (file for band B = prefixB.dat)
#   SOI solar line file name      'solar.h92'
#   SOI ILS lookup table file     'ils_tables_6816_L1B_1016pixels.dat'
#   SOI Optimal Sampling File Name 'optimal_sampling_ABSCO_conservative_'
#
# Local data path (from command line)
#   Sunrise and sunset file name  '20060914_sunrise_nadir.080'
#   '20060914_sunrise_nadir.080'
#   '20060914_sunrise_glint.080'
#   '20060914_sunrise_target_Bremen.080'
#   List of ECMWF profiles to process 'menus/ecmwf_profile_list.dat'
#   Colour slice file name        'menus/slices.oco'
#   File to hold output spectra    'output/test.hdf'
#

```

Table 5: A sample files menu.

`test.pro`, a binary file that contains the physical and optical properties (with the exception of the phase matrices) for the input profiles submitted to the radiative transfer code;

`test.nnn`, a binary file that contains the high resolution reflectance spectra for all profiles in OCO band `nnn`, where 001, 002 and 003 refer to the O₂ A-band, the weak CO₂ band and the strong CO₂ band respectively.

menus

Subdirectory `menus` contains menus that allow the user to configure the simulation. The default values in the menus may be edited interactively at run time while the user is debugging and testing, but for production runs the values specified in the menus can be accepted without consulting the user. This section lists the menus and outlines their contents, which for the most part are self-evident.

Files menu (FILES.MEN)

The files menu shown in table 5 specifies the shared data path and the names of key data files in that path. The name of the local data path is specified on the command line for the program, while the second half of the files menu specifies the names of key files in the local data path.

The menus are assumed to have two fields, a message field on the left-hand side that is fifty characters wide, and a value field on the right that also is fifty characters wide. When a menu is displayed on the screen, the user can move about the value field with the arrow and ENTER keys, over-typing the default values as required. Once the desired values have been set, the menu may be accepted with the key chord control-D. The modified menu will be written to the log file, creating a record of the selected options.

In the files menu, the file called ‘CO₂ file name’ is the subset of the PCTM global file for the orbit about to be simulated. In the example above, the file is for orbit number 8 and for nadir viewing. The ordering of the orbits begins at hour 00, minute 00 and second 00 on September 14, 2006. The CO₂ subset file must be created as a separate task before the simulator is run using the utility `extract_pctm`.

The file called ‘SOI endpoints file name’ in the files menu is the ASCII file that contains the wavelength limits of the three OCO bands. It is located in subdirectory SOI of the shared data path, and is read by the SOI code.

Similarly, the ‘SOI dispersion file name’ is the file containing dispersion parameters for each of the bands. The simulator assumes that the dispersion parameters for any band do not vary across that band, that there are 1016 pixels per band, and that the dispersion coefficients express the wavelength in terms of a pixel index that starts at 1 and runs to 1016. This conforms to the L1B specification that requires the four masked pixels at the end of each detector row to be excluded from the L1B product.

The colour stripe file name specified in the files menu points to an ASCII file that lists the positions (as pixel indices) of the colour stripes for each of the OCO bands.

The sunrise and sunset file nominated in the menu contains the times of sunrise and sunset for every orbit after a specified starting epoch. Here sunrise and sunset mean that the solar zenith angle at the target does not exceed a threshold, typically 80° and usually echoed in the extension of the file name. Both the starting epoch and the threshold are specified during creation of the sunrise and sunset file. Additionally, the user may specify a *lower* threshold in the configuration menu to be described later. The program (called `sunrise_sunset_program`) to generate sunrise and sunset files is under subversion control on the Colorado State University server `atlas.atmos.colostate.edu`. A copy may be checked out from the repository into a local directory (for example `sunrise`) with the command

```
svn co svn+ssh://atlas.atmos.colostate.edu/data/OCO/repository/sunrise_sunset/ sunrise
```

Finally, the name specified in the files menu for the file to hold output spectra is the name of the L1B file for the orbit. As explained earlier, the same file name, but with extensions `log`, `pro` and `nnn` will be used for the log file, the file containing the profiles, and the files containing the high-resolution reflectance spectra. All will be placed in the same directory.

Configuration menu (CONFIG.MEN)

The configuration menu shown in table 6 selects the various modes of operation of the simulator.

- (1) If ‘use Chevallier’s ECMWF profiles’ is set to true, then, rather than CloudSat and Calipso cloud profiles, meteorology and profiles of cloud water and cloud ice will be selected from the static data base of ECMWF profiles prepared by Chevallier (2001).

```

# CONFIGURATION MENU
# *****
#
# Use Chevallier's ECMWF profiles?          F
#   First ECMWF index to select (0 to use list) 0
#
# Use a uniform CO2 profile?                F
#   Default CO2 VMR (ppmv)                  380.000
#
# Force surface pressure?                   F
#   Surface pressure (atm)                   1.000
# Force surface height?                     F
#   Surface height (m)                      0.000
# Use polarized land BRDFs?                 F
# Force surface reflectance?                F
#   BRDF_Type (0/2 = Lambert/Cox-Munk+foam) 0
#     Lambertian surface albedo (A, W, S)    0.100 0.100 0.126 0.126 0.122 0.122
#     Surface wind speed (m/s)               5.000
# Use high-reflectivity ocean model?        F
# Force fixed geometry?                     F
# Force fixed position?                     F
# Force fixed polarization angle?           F
# Scan mode (0/1/2=nadir/glnt/target)      0
#
# Footprint angular width along slit axis (deg) 0.000
# Slit misalignment (A, W, S) (deg)         0.000 0.0000 0.000
#   0.0 0.0236 0.0
#
# Force random height variations             F
#   Maximum height variation (m) (A, W, S)  0.000 0.000 0.000
#
# Maximum allowed solar zenith angle (deg)  80.000
# Skip radiative transfer                   F
# Skip cloudy scenes?                       F
# Calipso aerosol? (T/F=old; only for CloudSat) F
# Random aerosol OD (only affects old aerosol)? T
# Use Old Aerosol Types (only for Calipso)? F
#
# List of reported soundings per frame      0 0 0 0 1 0 0 0
# Row scatter scale factor for colour slices 10
#
# Writing timing info to screen             F
#
# Seeds for the random number generator     1 2 3 4 5 6 7 8 9 0

```

Table 6: A sample configuration menu.

The satellite still will move along its orbit within the simulator, and the profile of CO₂ still will be extracted from the PCTM data base. However, the meteorology and profiles of cloud water and ice will be taken in sequence from Chevallier's data base, beginning with the profile index specified by the second line of the configuration menu. If the logical variable 'skip cloudy scenes' is set to false later in the configuration menu, then radiance spectra will be computed for all scenes from the data base. However, if the flag is true, then the frame quality flag for cloudy scenes in the L1B file will be set to zero, and dummy values will be assigned to the radiance spectra. This option makes for much faster simulations if only 'almost clear' scenes are required, because the radiative transfer is skipped for cloudy scenes.

- (2) If 'use Chevallier's ECMWF profiles' is set to false, then the vertical profiles of cloud water and ice and the corresponding effective radii will be taken from CloudSat data files. The meteorology will be extracted from ECMWF profiles collocated and simultaneous with the CloudSat observations. This ECMWF data is part of the CloudSat data distribution. When CloudSat deems that a profile is clear, meaning that the cloud water and cloud ice are below thresholds specified in the thresholds menu, described later, then the scene is 'almost clear'. The plan for the simulator is to derive the optical properties of the almost clear scenes from Calipso. However, at the time of writing, this has not been implemented, so as a temporary proxy the simulator scans through Chevallier's static ECMWF data base searching for profiles that meet the 'almost clear' criterion. Only the cloud water and cloud ice are taken from the ECMWF profile, and then they are interpolated to the CloudSat vertical grid. There is no attempt to match the selected profile to the latitude and longitude of the target.
- (3) If 'use a uniform CO₂ profile' is set to true, then the CO₂ VMR will be forced to the value set on the following line. Otherwise, the CO₂ VMR will be extracted from the PCTM data base for the time and location of the CloudSat data.
- (4) If 'force surface pressure' is set to true, then the surface pressure from the ECMWF data will be over-ridden by the value of surface pressure specified on the following line. Note that the surface pressure is specified in atmospheres, rather than Pa or hPa.
- (5) If 'force surface height' is set to true, then the surface height measured by CloudSat will be over-ridden by the value specified on the following line. The surface height is specified in metres, and is with respect to the reference ellipsoid.
- (6) The flag 'use BRDF rather than Lambertian albedo' allows the user to choose between the MODIS surface BRDF and a Lambertian albedo. However, because the BRDF is provided only for land surfaces, and the data often has gaps for regions frequently obscured by cloud, the simulator has back-up options for setting the surface albedo. First, if the Lambertian model has been selected, then the data base (also derived from MODIS) listed in the files menu will be used to interpolate the surface albedo from the MODIS bands to the OCO bands. Second, if a BRDF is requested, but the MODIS BRDF data files indicate missing data, then the selection will revert to the default Lambertian surface. Third, if the user sets the flag 'force surface albedo' to

true, then neither data base will be consulted; instead the simulator will assume the surface to be Lambertian and assign the albedos specified on the following line for the three OCO bands, with A/W/S denoting the O₂ A-band, the weak CO₂ band and the strong CO₂ band respectively. Two values are quoted for each band, being the Lambertian albedos at the endpoints of the band.

- (7) If ‘force fixed geometry’ is set to false, then the simulator will use the zenith angles and azimuths calculated by the orbit module for the OCO targets. However, if the flag is set to true, then a later menu (`GEOMETRY.MEN`) will be invoked asking the user to specify the geometry.
- (8) The scan mode (nadir, glint or target) is specified by 0, 1 or 2. While the position of the target in glint mode is calculated correctly, the code assigns cloud and meteorology from the CloudSat data base to the glint target, even though CloudSat actually observes the subsatellite point. More work is needed to remove this restriction.
- (9) Targets where the solar zenith angle exceeds the maximum specified in the menu are excluded from the output data files. To include all possible targets, the maximum solar zenith angle should be set to 90°.
- (10) Of the eight possible sounding positions, only those listed with ones in the ‘list of reported soundings per frame’ are included in the output data files. At present the spatial resolution of the meteorology and CO₂ profiles does not warrant including more than one sounding per frame, except for studies concerned with the impact of misalignment upon the spectra and retrieved X_{CO_2} . Similarly, the option of providing height differentials between the footprints is provided.
- (11) The colour slice data in the output L1B file is a place-holder, because the input data does not justify separate calculations for the twenty detector rows that are summed and reported in L1B files. The mean of the colour slices is set to the radiance calculated for the wavelength of the colour slice. The standard deviation of the rows contained in the colour slice is defined (arbitrarily) to be the ‘row scatter scale factor for colour slices’ times the radiance uncertainty, the latter derived from the instrument noise model.
- (12) Finally, the last line in the menu lists seeds for the random number generator. The number of seeds required depends on the compiler and the computer architecture. The simulator interrogates the random number generator to determine the number of seeds, and the result is written to the log file. The last line of the menu lists ten seeds; usually that will be sufficient.

Geometry menu (`GEOMETRY.MEN`)

If the user selects ‘force fixed geometry’ in the configuration menu, then a geometry menu, shown in table 7, will be displayed, allowing the user to specify fixed values for the zenith angles and azimuths of sun and satellite. The values specified in this menu will over-ride the values calculated using the orbit model.

```

# CONFIGURATION FOR FIXED GEOMETRY AND POSITION
# *****
#
# Solar zenith angle      (deg)          50.30981317D0
# Solar azimuth          (deg)          0.0D0
#
# Satellite zenith angle (deg)          0.0D0
# Satellite azimuth      (deg)          0.0D0
#
# Target latitude        (deg North)     53.0833D0
# Target longitude       (deg East)      8.8167D0
#
#   Saudia Arabia       23.07250000 N
#                       16.06143851 E
#
#   Bremen              53.0833 N
#                       8.8167 E
#
# Polarization angle    90.0D0
#
# Whether or not these values are used depends
# on the switches
#   ForceFixedGeometry,
#   ForceFixedPosition
# and
#   ForceFixedPolarizationAngle
# in the main configuration menu.
#

```

Table 7: A sample geometry menu.

```

# CLOUDSAT AND CALIPSO THRESHOLDS
# *****
#
# CloudSat min detectable cloud water (mg/m^3)    100
# CloudSat min detectable cloud ice   (mg/m^3)    5
#
# Almost clear liquid water threshold (g/m^2)     2.0
# Almost clear ice    water threshold (g/m^2)     10.0
#

```

Table 8: A sample threshold menu.

Threshold menu (THRESHOLD.MEN)

The threshold menu shown in table 8 sets the detectable limits of cloud water density and cloud ice density for CloudSat, in each case in units of mg m^{-3} . Cloud layers with less water or ice than the thresholds will be invisible to CloudSat. In addition, the thresholds menu sets the column densities of cloud water and ice that are deemed to correspond to ‘almost clear’ conditions. For the latter thresholds, the units are g m^{-2} .

Timing menu (ORBIT.MEN)

The orbit and timing menu shown in table 9 allows the user to specify the file containing the Keplerian elements of the orbit and timing parameters for the simulation.

- (1) The first option of the menu is the name of the file (in subdirectory `menus` of directory `dat_customized`) that contains the Keplerian elements of the orbit. The default presently uses the orbit of the CloudSat satellite.
- (2) The orbit model uses the second-order perturbation solution of the equations of orbital motion developed by Brouwer (1959), which shows that the argument of perigee and the right ascension of the ascending node precess with time. The rates of precession may be specified in the orbit file, but alternatively they may be calculated using second-order perturbation theory. Four options are offered:
 - (a) no adjustment, meaning use the rates of precession as specified in the orbital elements file;
 - (b) reset the rate of precession of the ascending node so that it precesses through 360° in exactly one year;
 - (c) use second-order perturbation theory to estimate the rates of precession of the argument of perigee and the right ascension of the ascending node, if that data is not available elsewhere;
 - (d) reset the rate of precession of the ascending node so that it precesses through 360° in exactly one year, and then require that the anomalistic period, inclination and rate of precession of the argument of perigee are consistent, at least to second-order in perturbation theory.

Generally the last option should be selected.

```

# TIMING PARAMETERS
# *****
#
# Satellite orbital elements file           'CLOUDSAT.orb'
#
# Element adjustment option                3
#   0: no adjustment
#   1: reset precession of ascending node
#   2: second-order perturbation
#   3: reset precession of ascending node +
#       second-order perturbation
#
# Orbit number                             8
#   African orbit nadir                    8
#   African orbit glint                    8
#   Target Bremen                          1
#
# Start at satellite epoch                  F
#
# Time step (s)                            2.000
# Number of frames                          10000
# Set the number of frames from sunset file? T
#

```

Table 9: A sample orbit and timing menu.

- (3) The user normally will run the simulation for the orbit nominated in the menu. If so, then data from the sunrise and sunset file will be used to determine the starting and ending times of the orbit. Alternatively, if the flag ‘start at satellite epoch’ is set to true, the simulation will start at the time at which the Keplerian elements of the orbit are specified. The latter information is found in the file containing the Keplerian elements.
- (4) The time step is the period between frames. Although OCO will sample with a third of a second between frames, the spatial resolution of the meteorological and CO₂ fields does not warrant such fine temporal resolution for the simulator. The default resolution (2s) is a reasonable compromise that is consistent with the spatial scales of the data and yet minimizes the computing time.
- (5) Finally, the simulation will continue until the number of frames collected is equal to the value specified in the orbit menu. However, if the the user specifies more frames than recorded for the nominated orbit in the sunrise and sunset file, then the simulation will terminate at the end of the orbit. Thus, entering a very large number forces the complete orbit to be simulated.

Keplerian elements menu

Generally the user will not need to modify the contents of the file containing the Keplerian elements of the orbit, shown in table 10. Updates only should be required for very long simulations; for simulations of a few days, the parameters may be considered to be fixed for

```

# ORBIT PARAMETERS (tweaked epoch)
# *****
#
# CLOUDSAT
#
# Satellite epoch (y/m/d)          2006  9 13
#                               (h/m/s/ms)    19 25  0  0
#
# Semi-major axis                  0.708067809E+07
# Eccentricity                     0.150900000E-03
# Mean anomaly                     0.221242300E+03
#
# Inclination of orbit             0.982109000E+02
# Argument of perigee              0.990523000E+02
# Right ascension of ascending node 0.198553000E+03
#
# Anomalistic period               0.988261795E+02
#
# Rate of precession perigee       0.000000000E+00
# Rate of precession ascending node 0.000000000E+00
#

```

Table 10: A sample Keplerian elements menu, in this case for CloudSat.

the purposes of the simulator. The Dundee Satellite Receiving Station provides a convenient source of the Keplerian elements for many satellites (<http://www.sat.dundee.ac.uk/>).

Radiative transfer menu (SOI.MEN)

The SOI menu shown in table 11 specifies parameters that are needed by the radiative transfer code. These parameters control the speed, accuracy, and other particulars of the radiative transfer solver. The first line of this file controls the basic verbosity of the solver (on/off). The next block of lines, each with two columns, controls parameters related to the monochromatic radiative transfer, when run in either low-accuracy (left column) or high-accuracy (right column) mode. The monochromatic radiative transfer returns Stokes' parameters I , Q and U at a particular wavelength for a pre-computed set of optical properties, and this monochromatic calculation has many parameters that control its speed and accuracy, the primary factors being the number of streams, the initial layer optical thickness and the level of polarization correction. For the latter, levels 0, 1 and 2 mean no polarization calculation ($Q = U = 0$), first-order and second-order of scattering polarization correction, respectively. Both the intensity-only code and the polarization code can model pseudo-spherical geometry. Some of the other general radiative transfer options are listed below; the remainder are self-explanatory.

Radiative transfer speedup method. Setting this option to zero will force a line-by-line calculation using the parameters for the 'low accuracy' (left-hand) column. Setting it to one will turn on the low-streams interpolator, a method of speeding up the radiance calculations, essentially by a line-by-line approach with the 'low accuracy' parameters followed by corrections with a handful of high-accuracy calculations. Setting the option to two currently

```

# SOI PARAMETERS
# *****
#
# Verbose driver output? T
# RT options: LO(1st col) HI(2nd col)
# Number of streams lo, hi 6 24
# Initial layer optical thickness (0 = auto) 3.0E-4 1.0E-5
# Apply delta scaling? T T
# Apply TMS single scattering correction? T T
# Pol correct (0/1/2=no/10S/20S)? 1 2
# Use truncated doubling? T F
# Use adding? F T
# Apply pseudo-spherical correction? T T
# Fractional convergence for SOI 2.0E-5 2.0E-5
# Fractional convergence for fourier loop 3.0E-5 3.0E-6
# Layer initialization (0/1/2=auto/EIGI/SSA) 0 0
# Verbose RT? F F
#
# RT speedup method (0/1/2=None/LSI/EOF) 1
# NSUM for 2+OS RT (LO only) 3
# Use optimal sampling? T
# Gas interpolation (0/1/2=avg/bdy/quadratic) 0
# Example LSI file name 'lsi_bounds1.txt'
#
# Output hi-res spectrum? (0=no, 1=txt, 2=binary) 0
# Output lo-res spectrum? F
# Output LSI files (if LSI on)? F
#
# Use Doppler shifts? F
# Force constant sun-earth distance? T
# Convolve with solar spectrum? T
# Solar continuum model (1=old;2=solspec fit) 1
# Cloud-free RT? F
#
# Bands to process (insert 0 to exclude) 1 2 3
# Number of channels per band 1016 1016 1016
# ILS type (0=Gaussian, 1=Table) 1
# Gaussian ILS FWHM values (nm) 0.042472 0.075820 0.097318
#

```

Table 11: A sample menu for the SOI radiative transfer code.

is experimental, and should not be used in general.

N_{sum} for 2+OS RT. The monochromatic radiative transfer calculates the first-order of scattering exactly (fast), and then approximates the contributions from multiple scattering. The latter calculations use a reduced vertical grid when $N_{sum} > 1$. For instance, if there are 60 vertical layers in the input profile, setting $N_{sum} = 3$ will force the multiple scattering calculations to use 20 layers instead. The optical properties are averaged in an intelligent way over sets of N_{sum} layers in order to maximize the accuracy of the resulting radiative transfer.

Use optimal sampling? Regardless of whether LSI is on or off, line-by-line calculations are performed for thousands of spectral points per OCO band. Sometimes, spectral points may be skipped and then estimated by linear interpolation from their neighbours. This option speeds up the radiative transfer by a factor of roughly two, with negligible loss in accuracy.

Gas interpolation. This controls the method used to interpolate from the pressure and temperature grid in the gas absorption table to the desired pressure and temperature. Option 0 is recommended, in which the mean pressure and temperature are calculated for a given layer, and a bilinear interpolation is performed to get the mean absorption coefficient for the layer. Option 1 does a bilinear interpolation at each layer boundary; this option is slightly less accurate than option 0. Option 2 is highly experimental, and should not be used.

Output hi-res spectrum? Setting this option to 1 will cause text files to be written for each profile and band, containing the results of the high-resolution radiative transfer calculation. These files also contain the column integrated gas optical depths for the band in question. Setting this to 2 will cause the high-resolution spectrum to be written into a common binary file (which contains all the spectra for all profiles and band). This latter option *does not work* when parallel computations are used.

Output lo-res spectrum? Setting this to true will cause the convolved radiance spectrum to be written for each profile and band. The header of the file contains extra information, such as particulars of the profile, geometry, radiative transfer options, calculation time, etc.

Output LSI files (if LSI on)? Setting this to true will cause a file to be written containing information on the low-streams interpolator activity for a particular profile and band. This is useful to see the degree of ‘interpolation’, and to debug problems with the LSI. In general this switch can be turned off.

Use Doppler shifts? Setting this switch to true enables both the sun-earth and earth-OCO Doppler shifts to be taken into account when computing the spectra. The Doppler velocities are calculated automatically by the simulator.

Force constant sun-earth distance? This option adjusts the strength of the solar spectrum by the inverse square of the solar distance. Setting it to true will use the mean sun-earth distance (1 astronomical unit); otherwise it will use the true sun-earth distance for the current day of the year.

Convolve with solar spectrum? If this switch is false, the solar spectrum is set to unity, so the code returns the reflectivity spectrum convolved with the OCO instrument response.

Solar continuum model. This parameter selects the solar continuum model. Model 1 is an older model that was used for most of the original algorithm testing, but is not realistic. Model 2 is based on a fit to observational data from SOLSPEC.

Cloud-free RT? Setting this to true ignores the effect of clouds and aerosols on the radiative transfer.

Bands to process. This line can be used to specify which bands should be processed. For all three bands, set this to '1 2 3'. For band 2 only, set this to '2 0 0', for bands 2 and 3, set it to '2 3 0', etc.

8.3 Distributing the simulator over the OCO cluster at CSU

Users may need to run the orbit simulator many times with different combinations of values for various parts of the menu files. To accomplish this task, the subversion repository includes a script, `launch_orbit`, that can create copies of the `dat_local` directory with the appropriate modifications to the menu files, and optionally submit runs to the Torque/PBS batch scheduling system on `ococluster.cira.colostate.edu`.

The `launch_orbit` script is located in the `src` directory. It uses the following syntax `launch_orbit [--no-run] <input file> <template dir> [target dir] [orbit executable]`. The script processes a list of runs from the input file and a template copy of the `dat_local` directory that contains variables which will change between runs. An example input file might appear as in table 12. Each RUN stanza contains a list of key/value pairs separated by equality signs. The keys are matched to variable names in any of the menu files, which are replaced by the values. For long lists of runs, the user typically writes a script to generate the input file.

The template menu files use a bash-style syntax: `${variable name[:default value]}`, that is, a dollar sign and curly braces that contain a variable name and, optionally, a default value separated by a colon. An example template menu file with variables might appear as in table 13.

For each RUN stanza of the input file, `launch_orbit` performs the following steps.

- (1) It makes a copy of the template directory (`dat_local`) with the same name as the run (the text in quotes after the keyword 'RUN'). This copy is created in the target directory. If the optional target directory is not specified at the command line, the copies are created in the current directory.

```

# Comments start with ah # and run to the end of a line
RUN "test001"
    SET_NUM_FRAMES = T
    TIME_STEPS=4
end

RUN "test002"
    SET_NUM_FRAMES = T
endrun

RUN "test003"
    SET_NUM_FRAMES = T
    ELEM_ADJ_OPT = 10
end run

RUN "test004"
    SET_NUM_FRAMES = F
    TIME_STEPS=7
    ELEM_ADJ_OPT = 17
end run "test004"

```

Table 12: A sample input file for the launch_orbit script.

```

# TIMING PARAMETERS
# *****
#
# Satellite orbital elements file           'CLOUDSAT.orb'
#
# Element adjustment option                ${ELEM_ADJ_OPT:3}
#   0: no adjustment
#   1: reset precession of ascending node
#   2: second-order perturbation
#   3: reset precession of ascending node +
#       second-order perturbation
#
# Orbit number                             8
#   African orbit nadir                    8
#   African orbit glint                    8
#   Target Bremen                          1
#
# Start at satellite epoch                  F
#
# Time step (s)                            ${TIME_STEPS:2}
# Number of frames                         10000
# Set the number of frames from sunset file? ${SET_NUM_FRAMES}
#

```

Table 13: A sample menu template with replaceable variables.

- (2) It replaces variables in each of the menu files with the appropriate value. The value is whatever value is listed in the stanza for that run from the input file. If the run's stanza does not contain that variable, `launch_orbit` uses the default value from the variable definition. If a variable doesn't supply a default value and the run's stanza doesn't contain that variable, `launch_orbit` stops execution with an error.
- (3) It submits a job to the Torque/PBS batch scheduling system that will run the simulator with the directory created for that run. The optional command line argument `--no-run` will cause `launch_orbit` to skip this final step.

9 Acknowledgements

This research was funded by JPL contract 1280999.

References

- Austin, R., 2007: Level 2B Radar-only cloud water content (2B-CWC-RO) process description document. http://www.cloudsat.cira.colostate.edu/ICD/2B-CWC/2B-CWC-RO_PD_5.1.pdf.
- Austin, R. T., and G. L. Stephens, 2001: Retrieval of stratus cloud microphysical parameters using millimeter-wave radar and visible optical depth in preparation for CloudSat 1. Algorithm formulation. *J. Geophys. Res.*, **106**, 28233–28242.
- Baum, B. A., 2007: <http://www.ssec.wisc.edu/~baum/Cirrus/IceCloudModels.html>.
- Baum, B. A., A. J. Heymsfield, P. Yang, and S. T. Bedka, 2005a: Bulk scattering properties for the remote sensing of ice clouds. Part I: microphysical data and models. *J. Appl. Meteorol.*, **44**, 1885–1895.
- Baum, B. A., P. Yang, A. J. Heymsfield, S. Platnick, M. D. King, Y.-X. Hu, and S. T. Bedka, 2005b: Bulk scattering properties for the remote sensing of ice clouds. Part II: narrowband models. *J. Appl. Meteorol.*, **44**, 1896–1911.
- Bodhaine, B. A., N. B. Wood, E. G. Dutton, and J. R. Slusser, 1999: On Rayleigh optical depth calculations. *J. Atmos. Oceanic Technol.*, **16**, 1854–1861.
- Bösch, H., G. C. Toon, B. Sen, R. A. Washenfelder, P. O. Wennberg, M. Buchwitz, R. de Beek, J. P. Burrows, D. Crisp, M. Christi, B. J. Connor, V. Natraj, and Y. L. Yung, 2006: Space-based near-infrared CO₂ measurements: Testing the Orbiting Carbon Observatory retrieval algorithm and validation concept using SCIAMACHY observations over Park Falls, Wisconsin. *J. Geophys. Res.*, **111**(D10), 23302.
- Bower, K. N., T. W. Choullarton, J. Latham, M. B. Baker, and J. Jensen, 1994: A parameterization of warm clouds for use in atmospheric general circulation models. *J. Atmos. Sci.*, **51**, 2722–2732.
- Breon, F.-M., 2008: Private communication.
- Brouwer, D., 1959: Solution of the problem of artificial satellite theory without drag. *Astronomical Journal*, **64**, 378–397.
- Chandrasekhar, S., 1950: *Radiative transfer*. Oxford Univ. Press, Oxford.
- Chevallier, F., 2001: Sampled databases of 60-level atmospheric profiles from the ECMWF analyses. SAF Programme Research Report 4, EUMETSAT/ECMWF, Am Kavaleriesand 31, Postfach D-64297 Darmstadt, Germany.
- Cox, C., and W. H. Munk, 1954a: The measurement of the roughness of the sea surface from photographs of the sun’s glitter. *J. Opt. Soc. Amer.*, **44**, 838–850.
- Cox, C., and W. H. Munk, 1954b: Statistics of the sea surface derived from sun glitter. *J. Mar. Res.*, **13**, 198–227.

- Dubovik, O., B. Holben, T. F. Eck, A. Smirnov, Y. J. Kaufman, M. D. King, D. Tanré, and I. Slutsker, 2002: Variability of absorption and optical properties of key aerosol types observed in worldwide locations. *J. Atmos. Sci.*, **59**, 590–608.
- Hansen, J. E., and L. D. Travis, 1974: Light scattering in planetary atmospheres. *Space Sci. Rev.*, **16**, 527–610.
- Heidinger, A. K., C. O’Dell, R. Bennartz, and T. Greenwald, 2006: The successive-order-of-interaction radiative transfer model. Part I: model development. *J. Appl. Meteorol. Clim.*, **45**, 1388–1402.
- Ivanova, D., D. L. Mitchell, W. P. Arnott, and M. Poellot, 2001: A GCM parameterization for bimodal size spectra and ice mass removal rates in mid-latitude cirrus clouds. *Atmospheric Research*, **59-60**, 89–113.
- Kawa, S. R., D. J. Erickson, S. Pawson, and Z. Zhu, 2004: Global CO₂ transport simulations using meteorological data from the NASA data assimilation system. *J. Geophys. Res.*, **109**(D18), 18312.
- Koepke, P., 1984: Effective reflectance of oceanic whitecaps. *Appl. Opt.*, **23**, 1816–1824.
- Lenoble, J., Ed., 1985: *Radiative transfer in scattering and absorbing atmospheres: standard computational procedures*. A. Deepak Publishing, Hampton, Virginia USA.
- Li, X., and A. H. Strahler, 1992: Geometric-optical bidirectional reflectance modeling of the discrete-crown vegetation canopy: effect of crown shape and mutual shadowing. *IEEE Trans. Geosci. Remote Sens.*, **30**, 276–292.
- Mishchenko, M., 2000: Private communication, mmishchenko@giss.nasa.gov.
- Monahan, E. C., and I. ÓMuircheartaigh, 1980: Optimal power-law description of oceanic whitecap coverage dependence on wind speed. *J. Phys. Oceanogr.*, **10**, 2094–2099.
- Nakajima, T., and M. Tanaka, 1988: Algorithms for radiative intensity calculations in moderately thick atmospheres using a truncation approximation. *J. Quant. Spectrosc. Radiat. Transfer*, **40**, 51–69.
- Natraj, V., R. J. D. Spurr, H. Boesch, Y. Jiang, and Y. L. Yung, 2007: Evaluation of errors from neglecting polarization in the forward modeling of O₂ A band measurements from space, with relevance to CO₂ column retrieval from polarization-sensitive instruments. *J. Quant. Spectrosc. Radiat. Transfer*, **103**, 245–259.
- O’Brien, D. M., and A. J. Prata, 1990: Navigation of ERS-1 along-track scanning radiometer ATSR images. *ESA Journal*, **14**, 447–465.
- O’Dell, C. W., 2009: Acceleration of multiple-scattering, hyperspectral radiative transfer calculations via low-streams interpolation. submitted to *J. Geophys. Res.*
- O’Dell, C. W., A. K. Heidinger, T. Greenwald, P. Bauer, and R. Bennartz, 2006: The successive-order-of-interaction radiative transfer model. Part II: model performance and applications. *J. Appl. Meteorol. Clim.*, **45**, 1403–1413.

- Palmer, K. F., and D. Williams, 1974: Optical properties of water in the near infrared. *J. Opt. Soc. Amer.*, **64**, 1107–1110.
- Peck, E. R., and K. Reeder, 1972: Dispersion of air. *J. Opt. Soc. Amer.*, **62**, 958–962.
- Polonsky, I., and D. M. O’Brien, 2009: OCO algorithm theoretical basis document. the ‘golden pairs’ apparent optical path difference (AOPD) retrieval algorithm. Technical report, Colorado State University.
- Rothman, L. S., D. Jacquemart, A. Barbe, D. Chris Benner, M. Birk, L. R. Brown, M. R. Carleer, C. Chackerian, K. Chance, L. H. Coudert, V. Dana, V. M. Devi, J.-M. Flaud, R. R. Gamache, A. Goldman, J.-M. Hartmann, K. W. Jucks, A. G. Maki, J.-Y. Mandin, S. T. Massie, J. Orphal, A. Perrin, C. P. Rinsland, M. A. H. Smith, J. Tennyson, R. N. Tolchenov, R. A. Toth, J. Vander Auwera, P. Varanasi, and G. Wagner, 2005: The HITRAN 2004 molecular spectroscopic database. *J. Quant. Spectrosc. Radiat. Transfer*, **96**, 139–204.
- Shettle, E. P., and R. W. Fenn, 1979: Models for the aerosols of the lower atmosphere and the effects of humidity variations on their optical properties. Technical report Environmental research papers, No. 676, AFGL-TR-79-0214, Air Force Geophysics Laboratory, Hanscom Air Force Base, Massachusetts 01731.
- Toth, R. A., L. R. Brown, C. E. Miller, V. Malathy Devi, and D. C. Benner, 2008: Spectroscopic database of CO₂ line parameters: 4300–7000 cm⁻¹. *J. Quant. Spectrosc. Radiat. Transfer*, **109**, 906–921.
- van de Hulst, H. C., 1957: *Light scattering by small particles*. Wiley, New York.
- Wanner, W., A. H. Strahler, B. Hu, P. Lewis, J.-P. Muller, X. Li, C. L. B. Schaaf, and M. J. Barnsley, 1997: Global retrieval of bidirectional reflectance and albedo over land from EOS MODIS and MISR data: theory and algorithm. *J. Geophys. Res.*, **102**, 17143–17161.
- Whitlock, C. H., D. S. Bartlett, and E. A. Gurganus, 1982: Sea foam reflectance and influence on optimum wavelength for remote sensing of ocean aerosols. *Geophys. Res. Lett.*, **9**, 719–722.
- Wiscombe, W., 1977: The delta-M method: rapid yet accurate radiative flux calculations for strongly asymmetric phase functions. *Journal of Atmospheric Sciences*, **36**, 1408–1422.